Applied Catalysis B: Environmental 343 (2024) 123550

Contents lists available at ScienceDirect

Applied Catalysis B: Environmental

journal homepage: www.elsevier.com/locate/apcatb

# A review of mechanistic insights into $CO_2$ reduction to higher alcohols for rational catalyst design

Yao Sheng [a,b], Mikhail V. Polynski [c], Mathan K. Eswaran [c], Bikun Zhang [c], Alvin M.H. Lim [c], Lili Zhang [d], Jianwen Jiang [c], Wen Liu [a,b,*], Sergey M. Kozlov [c,**]

[a] School of Chemistry, Chemical Engineering and Biotechnology, Nanyang Technological University, 62 Nanyang Drive, Singapore 637459, Singapore
[b] Cambridge Centre for Advanced Research and Education, 1 CREATE Way, Singapore 138602, Singapore
[c] Department of Chemical and Biomolecular Engineering, National University of Singapore, 4 Engineering Drive 4, Singapore 117585, Singapore
[d] Institute of Sustainability for Chemicals, Energy and Environment (ISCE2), Agency for Science, Technology and Research, A*STAR, 1 Pesek Rd, Singapore 627833, Singapore

ARTICLE INFO

*Keywords:*
$CO_2$ reduction
Catalysis
Alcohols
Oxygenates
Reaction mechanism

ABSTRACT

The utilization of captured $CO_2$ for chemical synthesis could play an important role in reducing $CO_2$ emissions. Higher alcohols stand out among various products of $CO_2$ reduction due to high market prices and diverse applications, e.g., as fuel additives. However, developing catalysts for this reaction requires a profound understanding of the reaction mechanisms and catalyst design principles, which are discussed in the present review. Depending on the catalytic sites, higher alcohol synthesis could proceed via vastly different pathways. Herein, we outline how various proposed reaction mechanisms lead to different catalyst design strategies for optimizing the rate of $CO_2$ conversion into reactive $C_1$ intermediates (CO, $CH_x$, $CH_xO$, and HCOO) and their coupling into $C_{2+}$ intermediates that are eventually converted into higher alcohols. Lastly, we discuss knowledge gaps in achieving rational catalyst design for higher alcohol synthesis and the breakthrough potential of machine-learning techniques for catalyst discovery.

## 1. Introduction

For a long time, $CO_2$ has been used as a carbon source in the chemical industry to produce a variety of societally important chemicals such as methanol [1], urea [2], and various carbonates [3]. Currently, extending the utilization of $CO_2$ feedstock to produce more diverse sustainable fuels and chemicals (i.e., the $CO_2$ capture and utilization scheme, also known as CCU) is considered an important pillar in the global effort to reduce atmospheric $CO_2$ emissions [4,5]. Moreover, $CO_2$ conversion to chemicals will play a major role in closing the carbon cycle in a circular economy, which aims to reuse the captured $CO_2$ instead of emitting or storing $CO_2$ in the environment [6]. Currently, substantial scientific attention is focused on developing technologies for either thermal [7], electrochemical [8], photocatalytic [9], or photothermal [10] $CO_2$ reduction. Among those technologies, thermocatalytic $CO_2$ reduction is the closest to large-scale deployment. However, thermocatalytic $CO_2$ reduction can be considered sustainable only if it is facilitated by green $H_2$, whose production does not involve $CO_2$ emissions [11,12]. Besides the performance of the catalytic process itself, the economic feasibility of $CO_2$ reduction technologies also strongly depends on the market price of the obtained products [13,14]. In particular, $CO_2$ reduction to higher alcohols is a promising CCU pathway owing to the relatively high price of the products and their potential application as fuel blends [15,16], which translates to great market volume and societal impact. For direct hydrogenation of $CO_2$ in a single reactor, the target higher alcohols (HAs) typically include $C_2$–$C_4$ linear alcohols (e.g., ethanol, *n*-propanol, and *n*-butanol), while isomeric and $C_{5+}$ alcohols could be prepared from the $C_2$–$C_4$ linear alcohols via further chemical conversion steps (e.g., aldol condensation) [17,18]. The present review focuses on the one-step conversion of $CO_2$ to $C_2$–$C_4$ linear alcohols, thereafter, referred to as HAs. To date, alcohols are primarily produced from fossil fuel feedstocks or through biological processes, with no commercial process for HA synthesis from $CO_2$ has been deployed so far. However, techno-economic analysis shows that alcohol synthesis from $CO_2$ and

* Corresponding author at: School of Chemistry, Chemical Engineering and Biotechnology, Nanyang Technological University, 62 Nanyang Drive, Singapore 637459, Singapore.
** Corresponding author.
*E-mail addresses:* wenliu@ntu.edu.sg (W. Liu), cheserg@nus.edu.sg (S.M. Kozlov).

https://doi.org/10.1016/j.apcatb.2023.123550

Available online 23 November 2023
0926-3373/© 2023 Elsevier B.V. All rights reserved.

green hydrogen could be economically feasible if the separation of alcohols from other reaction byproducts is efficiently achieved [19,20]. However, most alcohols are currently produced from biomass, posing additional challenges for scaling up, adding strains to land and water resources, and threatening food production [21,22].

$CO_2$ conversion to HA is a more complex process than more established CO hydrogenation to HA [23–26]. One of the key advantages of using $CO_2$ instead of CO as a feedstock for higher alcohol synthesis is its abundance, low cost, lower toxicity, and renewable nature. However, due to its high stability, transforming $CO_2$ into other chemicals often requires substantial energy or electro-reductive processes. In addition, compared to CO conversion, $CO_2$ hydrogenation produces more water, which is an undesired side-product that may accelerate catalysts deactivation through active component sintering [27,28]. Most importantly, $CO_2$ activation generates a wide variety of $C_1$ intermediates, which could be coupled to form $C_{2+}$ alcohols through a complex and diverse reaction network (as discussed below), whereas CO hydrogenation to HA is thought to proceed via the CO insertion mechanism [29–31].

Thus, one of the main challenges for $CO_2$ reduction to HA is the low yield or selectivity of the currently available catalysts, which have been covered in recent reviews [32–35]. In particular, much effort has been devoted to developing catalysts based on Rh, Co, Cu, Fe, Mo, $InO_x$, and their combinations (Tables 1 and 2) [23,36–72]. Typically, higher alcohol synthesis by $CO_2$ hydrogenation is performed at 200–380 °C, 0.1–10 MPa, an $H_2/CO_2$ ratio of 3, and gas hourly space velocity (GHSV) between 2200 and 36000 $h^{-1}$ in continuous flow fixed-bed reactors. However, some higher alcohol synthesis reactions were also performed in tank reactors, where typical reaction conditions used were 100–250 °C, 1–8 MPa, and an $H_2/CO_2$ ratio of 3. Moving forward, the discovery of novel catalysts for higher alcohol synthesis from $CO_2$ will likely involve rational catalyst design [73,74] and high-throughput experimentation accelerated by machine-learning techniques [75]. The efficiency and breakthrough in further studies will strongly depend on the understanding of the reaction mechanisms and structure-property relations in the prepared catalysts. Indeed, high-throughput experimental or computational catalyst screening can succeed only if it focuses on the most important catalyst features and reaction steps owing to the incredible complexity of the $CO_2$ reduction reaction network (Fig. 1),

**Table 1**
Catalytic performance of noble metal catalysts for higher alcohol synthesis from $CO_2$ hydrogenation.

| Catalyst [Ref.] | GHSV[a] ($h^{-1}$) | P[b] (MPa) | T[c] (°C) | $CO_2$ conv. (%) | HA sel. (%) | Space-time-yield |
|---|---|---|---|---|---|---|
| Rh-0.3$VO_x$/MCM-41 [36] | 6000 | 3 | 250 | 12 | 24 | 1.04 mmol $g^{-1}$ $h^{-1}$ |
| Rh/$SiO_2$[37] | 6000 | 5 | 240 | 7 | 15.5 | – |
| $Rh_1$/$CeTiO_x$ [38] | Tank | 1 | 250 | 6.3 | 99.1 | 0.26 mg $g^{-1}$ $h^{-1}$ |
| RhFeLi/$TiO_2$ [39] | 6000 | 3 | 250 | 15.7 | 35.9 | 63 mg $g^{-1}$ $h^{-1}$ |
| 2%Rh–2.5% Fe/$TiO_2$ [40] | 8000 | 2 | 270 | 9.2 | 6.4 | – |
| KFeRh-$SiO_2$ [41] | 7000 | 7.5 | 250 | 18.4 | 16 | 52.1 mg $g^{-1}$ $h^{-1}$ |
| $Pd_2$/$CeO_2$[42] | 3000 | 3 | 240 | 9.2 | 99.2 | 59.3 mg $g^{-1}$ $h^{-1}$ |
| $Pd_2Cu$ NPs/P25[43] | Tank | 3.2 | 200 | – | 92 | 41.5 mmol $g^{-1}$ $h^{-1}$ |
| Pd/$Fe_3O_4$[44] | 8000 | 3 | 300 | 2.9 | 48.2 | – |
| Pt/$Co_3O_4$[45] | Tank | 8 | 200 | – | 82.5 | 0.42 mmol $g^{-1}$ $h^{-1}$ |
| Pt/$Co_3O_4$-p [46] | 6000 | 2 | 200 | 22.4 | 4.1 | 0.56 mmol $g^{-1}$ $h^{-1}$ |
| Au/a-$TiO_2$ [47] | Tank | 6 | 200 | – | > 99 | 2.8 mmol $g^{-1}$ $h^{-1}$ |
| $Ir_1$−$In_2O_3$[48] | Tank | 6 | 200 | – | 99.7 | 0.99 mmol $g^{-1}$ $h^{-1}$ |

[a] Gas hourly space velocity in a fixed-bed reactor;
[b] Pressure;
[c] Temperature.

**Table 2**
Catalytic performance of non-noble metal catalysts for higher alcohol synthesis from $CO_2$ hydrogenation.

| Catalyst [Ref.] | GHSV[a] ($h^{-1}$) | P[b] (MPa) | T[c] (°C) | $CO_2$ conv. (%) | HA sel. (%) | Space-time-yield |
|---|---|---|---|---|---|---|
| 2.5K5Co-$In_2O_3$ [49] | 2250 | 4 | 380 | 35 | 29 | 169.6 mg $g^{-1}$ $h^{-1}$ |
| Na–Co/$SiO_2$[50] | 4000 | 5 | 250 | 18 | 62 | – |
| Co/$La_4Ga_2O_9$[51] | 3000 | 3.5 | 270 | 4.6 | 34.7 | – |
| Na–$Co_2C$ (111) [52] | 6000 | 5 | 310 | 53.2 | 17.5 | 72.5 mg $g^{-1}$ $h^{-1}$ |
| $Co_2C$\|\|CuZnAl [53] | 12000 | 5 | 250 | 20.7 | 16.4 | 2.2 mmol $g^{-1}$ $h^{-1}$ |
| $CoAlO_x$-600[54] | Tank | 4 | 140 | – | 92.1 | 0.4 mmol $g^{-1}$ $h^{-1}$ |
| $Co_{0.52}Ni_{0.48}AlO_x$ [55] | Tank | 4 | 200 | – | 85.7 | 1.3 mmol $g^{-1}$ $h^{-1}$ |
| $Co_3O_4$-m[56] | 6000 | 2 | 200 | 27 | 20 | 1.6 mmol $g^{-1}$ $h^{-1}$ |
| Co/$La_2O_3$-$La_4Ga_2O_9$[57] | 3000 | 3 | 240 | 9.8 | 65.8 | – |
| $Mo_1Co_{0.3}K_{0.9}$/AC [58] | 3000 | 5 | 320 | 23.7 | 6.7 | – |
| Na–CuCo-9[59] | 5000 | 4 | 330 | 22.1 | 58 | 80.8 mg $g^{-1}$ $h^{-1}$ |
| Cs-$Cu_{0.8}Fe_{1.0}Zn_{1.0}$ [23] | 4500 | 5 | 330 | 36.6 | 19.8 | 1.4 mmol $g^{-1}$ $h^{-1}$ |
| Na-Fe@C/K-CuZnAl[60] | 4500 | 5 | 320 | 39.2 | 35.0 | – |
| KFeCu/a-$ZrO_2$ [61] | 12000 | 4 | 320 | 25.7 | 26.1 | 125 mg $g^{-1}$ $h^{-1}$ |
| $Zr_{12}$-bpdc-CuCs [62] | Tank | 2 | 100 | 96 | > 99 | – |
| SKCuFeZn/CuZnAlZr[63] | 12000 | 5 | 320 | 36.6 | 18.2 | 173.9 mg $g^{-1}$ $h^{-1}$ |
| CuZnAl/K-CuMgZnFe[64] | 6000 | 5 | 320 | 42.3 | 20.2 | 106.5 mg $g^{-1}$ $h^{-1}$ |
| 4.6K-CuMgZnFe [65] | 6000 | 5 | 320 | 30.4 | 22.8 | 69.6 mg $g^{-1}$ $h^{-1}$ |
| Cu@Na-Beta[66] | 12000 | 1.3 | 300 | 7.9 | 69.5 | 5.6 mmol $g^{-1}$ $h^{-1}$ |
| PCN-224-Cu[67] | Tank | 1 | 130 | 74 | 100 | 4.5 mmol $g^{-1}$ $h^{-1}$ |
| Cu/$Co_3O_4$-2h[68] | 36000 | 0.1 | 350 | 13.9 | 16.3 | 86 mg $g^{-1}$ $h^{-1}$ |
| CuZnK/CuFeCoK [69] | 5000 | 6 | 350 | 32.4 | 21.6 | 72.4 mg $g^{-1}$ $h^{-1}$ |
| FeIn/Ce-$ZrO_2$[70] | 4500 | 10 | 300 | 29.6 | 28.7 | 96.6 mg $g^{-1}$ $h^{-1}$ |
| Fe/$Mo_2C$[71] | Tank | 4 | 200 | 10 | 16 | – |
| FeNaS-0.6[72] | 8000 | 3 | 320 | 32 | 16.1 | 80.5 mg $g^{-1}$ $h^{-1}$ |

[a] Gas hourly space velocity in a fixed-bed reactor;
[b] Pressure;
[c] Temperature.

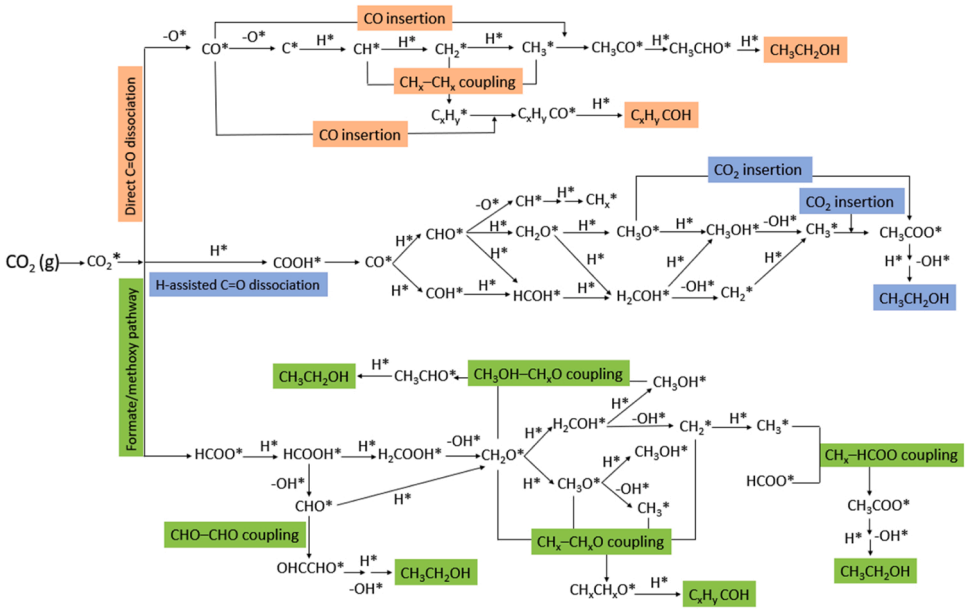


**Fig. 1.** Summary of possible pathways of $CO_2$ hydrogenation to higher alcohols. Throughout the text, * indicates adsorbed species.

similar to that of the electrochemical conversion of $CO_2$ to $C_{2+}$ species [76].

In this review, we critically analyze the mechanistic aspects of recent experimental and computational studies of $CO_2$ reduction to HA to elucidate structure-function relationships and propose catalyst design strategies for the future development of better catalysts for this reaction. We discuss various strategies to promote the reaction steps that are likely to be essential for the catalytic activity, e.g., the activation of $CO_2$ and $H_2$ reactants, and selectivity, e.g., the hydrogenation of the carbon center and C–C coupling. The latter reaction is shown to involve $CO_2$, CO, $CH_x$, or HCOO intermediates, depending on the nature of the catalyst. The great variety of C–C coupling pathways opens abundant opportunities for catalyst engineering but also makes it challenging to generalize catalyst design principles that apply to all types of catalysts. Both experimental and computational efforts in investigating the catalytic mechanisms are reviewed. We conclude the review by suggesting future research directions and the use of advanced catalyst design tools, such as machine learning algorithms, for the discovery and development of new catalysts for $CO_2$ reduction to higher alcohols.

## 2. Mechanism of $CO_2$ hydrogenation to higher alcohols

### 2.1. Dissociative adsorption and spillover of hydrogen

The availability of hydrogen adatoms is the prerequisite to the hydrogenation of $C_1$ building blocks and $C_2$ intermediates, as depicted in Fig. 1. In $CO_2$ hydrogenation reactions, catalysts can facilitate hydrogen dissociation by providing suitable adsorption sites for $H_2$ molecules and promoting their splitting into reactive hydrogen species. The dissociated hydrogen atoms can help to break the strong carbon-oxygen bonds in

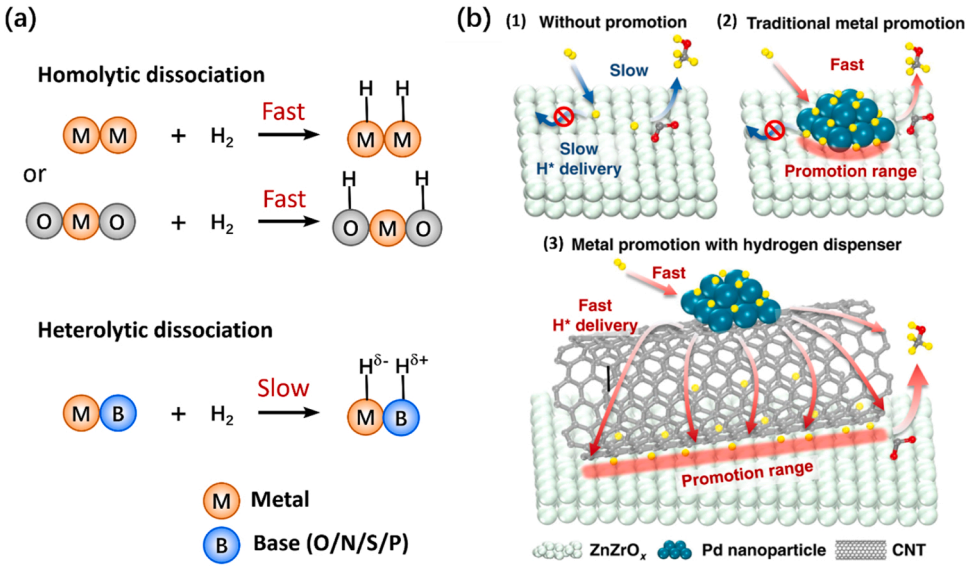


**Fig. 2.** (a) Illustration of $H_2$ dissociation pathways. (b) Schematic representation of H spillover engineering for $CO_2$ hydrogenation to methanol. (1) $ZnZrO_x$ catalyst without any metal promotion. (2) Pd-supported $ZnZrO_x$ catalyst: traditional metal/oxide catalyst utilizing metal promotion. (3) Pd/CNT + $ZnZrO_x$ catalyst: innovative catalyst system introducing metal promotion and hydrogen dispersion concept.
(a) Adapted with permission from Ref.[78]. (b) Adapted with permission from Ref.[86].

$CO_2$, initiating a series of subsequent reactions that lead to the formation of desired hydrocarbon products.

As shown in Fig. 2a, the mechanisms for the adsorption and dissociation of $H_2$ vary across different types of active sites and generally proceed via two distinct pathways: (i) homolytic dissociation, which occurs on transition metals and reducible metal oxides, leading to the formation of two hydride (M–H) or two hydroxyl (O–H) groups simultaneously, and (ii) heterolytic dissociation, taking place on metal–base pairs (base = O, S, N, P), resulting in the formation of hydroxyl (H adatom on base site) and hydride (H adatom on metal site) species [77,78]. In general, the homolytic activation of $H_2$ and the spillover of H from transition metals to oxides are kinetically fast and tend not to be the rate-limiting steps in hydrogenation reactions [60,79,80], whereas a slower rate of heterolytic $H_2$ dissociation may negatively affect $CO_2$ reduction kinetics [78,81]. The pathway and rate of $H_2$ dissociation significantly affect the reaction equilibrium, thus regulating the conversion of $CO_2$ [82,83].

Since $CO_2$ hydrogenation tends to occur across metal-support interfaces [61,84], H spillover rate is crucial for $CO_2$ reduction kinetics. Ling et al.[85] prepared $Pd_3Cu$ nanoparticles confined in a Zr-based metal-organic framework (MOF), namely UiO-66, to render close proximity between $CO_2$ and $H_2$ activation sites. Such proximity enabled a sufficiently fast rate of hydrogen spillover from $Pd_3Cu$ to surrounding oxidized Zr clusters and facilitated the facile formation of HCOO* from adsorbed $CO_2$. The hydrogen spillover mechanism was also found to be important on $Zr_{12}$ cluster of UiO-67 [62], which could catalyze $CO_2$ hydrogenation via a methanol formation cycle and an ethanol formation cycle. In both cycles, $H_2$ is activated on the $Cu^{2+}$ sites and spilled over to attack the neighboring carbon centers. Thus, there is a need to design catalysts with high surface densities of interfacial sites, e.g., by increasing the metal dispersion, such that the overall rate of $CO_2$ hydrogenation can be enhanced. When the active centers for $H_2$ activation and $CO_2$ reduction are spatially separated, hydrogen spillover can be facilitated by engineering channels for H diffusion within the catalyst. For example, carbon nanotubes (CNT) can form an efficient network for the distribution of hydrogen from metal nanoparticles to the active sites on oxide surfaces to increase the $CO_2$ reduction activity of Pd/CNT/$ZnZrO_x$ catalysts (Fig. 2b) [86].

In addition to affecting the rate of $CO_2$ hydrogenation, $H_2$ activation and the subsequent spillover could also influence product selectivity. For instance, the adsorption strength H* on the metal sites would govern its surface coverage, which subsequently influences the degree of hydrogenation and the selectivity of the catalysts towards $C_1$ products versus $C_{2+}$ products. The adsorption strength of the H adatoms can be tuned by controlling the particle size of the metals or chemical modification (e.g., doping). For example, Luk and co-workers [87] found that the confinement effect of conical carbon nanofibers with appropriately sized channels enables the formation of numerous Cu particles of moderate sizes and hinders the dispersion of the Fe phase in Cu-Fe catalysts, which limits the $H_2$ activation by Fe. Such architecture results in lower Fischer-Tropsch catalyst activity, ultimately leading to higher selectivity of the catalysts towards HA. The same researchers also uncovered K-doping as an effective means to increase the size of the Fe particles further, enhancing the proximity of Fe to Cu and increasing the selectivity toward HA up to 47%. K doping was also found to be an effective approach to modulating the adsorption strength of $H_2$. Xu et al. showed that incorporating K promoter into CuFe supported on the bimodal porous silica can enhance the CO chemisorption and moderate the $H_2$ chemisorption, thus improving carbon chain growth and enhancing the selectivity towards HA [88,89]. Moreover, Ding et al.[90] observed that the addition of K to CuFeZnMnO facilitated the migration of Fe from the bulk to the surface of the material, thereby increasing the ratio of surface Fe/Cu. As a result, K doping strengthened CO chemisorption and weakened $H_2$ chemisorption, affording a maximum HA selectivity of 31% at a K doping content of 0.5%. Moreover, $H_2$ could also be dissociatively activated by external stimuli such as non-thermal plasma (NTP), which can generate high-energy electrons in a discharge zone at ambient temperature and pressure without a catalyst. For instance, Zou et al. used NTP to achieve $CO_2$ hydrogenation to ethanol at ambient temperature and pressure on partially reduced HKUST-1 [91].

In summary, despite often being considered kinetically facile and mechanistically trivial, the dissociative activation of $H_2$ and the subsequent spillover are vital in determining both reaction rates and product selectivity. The rate of $H_2$ activation is highly dependent on the catalyst composition, promoter, and type of support. Additionally, hydrogen spillover enables the efficient delivery of hydrogen species from adjacent metal sites to adsorbed $CO_2$, which is eventually hydrogenated to HA.

### 2.2. $CO_2$ activation

The formation of higher alcohols involves the coupling of $C_1$ building blocks (viz. oxygenates and alkyl species), which are produced by $CO_2$ hydrogenation. The commonly accepted $CO_2$ activation mechanisms for higher alcohol synthesis catalysts include: (i) the CO-mediated pathway, which involves two steps: the conversion of $CO_2$ to CO and the subsequent hydrogenation and/or dissociation of CO, and (ii) the formate/methoxy-mediated pathway, where the $CO_2$ reacts with hydrogen to form $C_1$ intermediates including formate (HCOO*) and/or methoxy ($CH_3O$*) species [36,50,51].

#### 2.2.1. CO-mediated pathway

In the CO-mediated pathway, the formation of CO* can proceed via $CO_2$ dissociation through the direct cleavage of one C═O bond in $CO_2$ ($CO_2$* → CO* + O*) or H-assisted C═O dissociation ($CO_2$* + H → COOH*→CO* + OH*). The CO-mediated mechanism for $CO_2$ reduction to ethanol was first proposed by Kusama et al. for the Rh/$SiO_2$ catalyst based on their experimental observation of CO* in Fourier transform infrared (FTIR) spectroscopy [37]. Direct $CO_2$ dissociation is common on oxide surfaces with abundant O vacancies, which can be rapidly filled by the O* species formed upon dissociation. In turn, the produced CO* would be transformed into CH* by hydrogenation. For example, Lou et al. [42] prepared $CeO_2$-supported Pd dimers ($Pd_2/CeO_2$), which catalyzed direct C═O cleavage with a barrier of 0.7 eV. The formation of HCOO* and COOH* from $CO_2$ in the H-assisted pathway on this catalyst required overcoming much higher activation barriers of 1.72 eV and 1.80 eV, respectively, suggesting that C═O bond in $CO_2$ would preferentially undergo direct C═O bond dissociation on Pd dimers to form CO* as the first step in $CO_2$ activation (Fig. 3a). In contrast, the $CO_2$ hydrogenation to formate (HCOO*) and carboxyl (COOH*) is thought to be the main $CO_2$ activation pathway on Pd single atoms and Pd particles supported on $CeO_2$ [43,44,92,93]. DFT calculations also reveal the direct dissociation of $CO_2$ to CO* on pristine and Ir-promoted $In_2O_3$ catalysts for $CO_2$ hydrogenation to ethanol [48]. Note that Ir dopants in $In_2O_3$ promote not only $CO_2$ dissociation but also $CO_2$ chemisorption by forming unique active site structures.

The H-assisted $CO_2$ dissociation pathway is also prevalent on many catalysts, proceeding through the formation of COOH* followed by its dihydroxylation to form CO* and OH* (also known as the COOH-mediated pathway). *In situ* diffuse reflectance infrared Fourier transform spectroscopy (DRIFTS) studies by Liang et al. [96] found that the exposure of single-atom Co/SBA-15 catalyst to $CO_2$ and $H_2$ generated CO* through the H-assisted dissociation of $CO_2$ without the formation of formate or carbonate intermediates. C═O bond activation in $CO_2$ was also achieved by non-thermal plasma (NTP). Such an approach is particularly beneficial to catalysts with weak $CO_2$ adsorption but strong CO adsorption, such as partially reduced HKUST-1. In the plasma discharge zone, $CO_2$ could also be activated to carboxylate COO* and further dissociate to CO* or undergo hydrogenation to HCOO* , as observed by in situ DRIFTS spectroscopy [91].

The adsorbed CO can further react either through direct CO dissociation to generate a carbon atom (C*) or through H-assisted CO

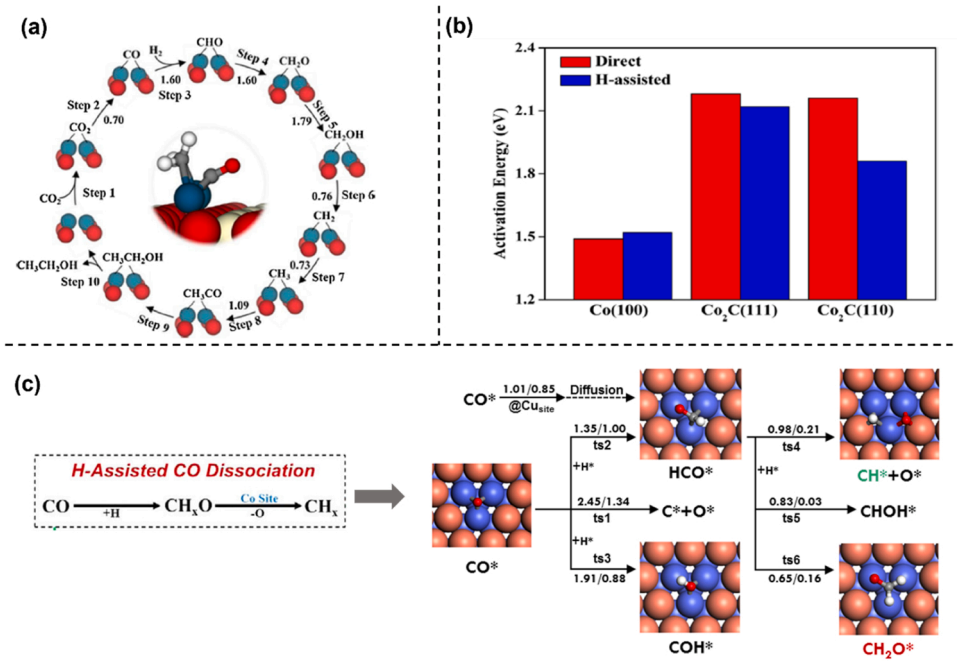


**Fig. 3.** (a) Activation barriers (in eV) of elementary steps involved in the catalytic cycle for the formation of ethanol over $Pd_2/CeO_2(110)$. [42]. (b) Activation energies (in eV) of direct (red) and H-assisted (blue) CO activation pathways on fcc Co(100), Co-terminated (111) and (110) surfaces of $Co_2C$. [94]. (c) Formation of $CH_x$ species for C–C coupling from hydrogenation and dissociation of CO on the $Cu_6Co_3$ surface (small gray, C; small red, O; small white, H). [95].
(a) Adapted with permission from Ref. [42] (b) Adapted with permission from Ref.[94]. (c) Adapted with permission from Ref.[95].

dissociation to form formyl (CHO*) and/or isoformyl (COH*) species. For instance, Pei et al. [94] concluded that during CO activation on Co-$Co_2C$ catalysts, noble-metal-like $Co_2C$ was responsible for the non-dissociative adsorption of CO, while metallic Co provided sites for dissociative CO adsorption and subsequent carbon-chain growth (Fig. 3b). Importantly, the interface between the cobalt metal and its carbide phase was found essential for efficient alcohol synthesis. The alloying of Co catalysts with Cu was also found to suppress direct dissociation of the C≡O bond, although it still enabled the H-assisted CO dissociation mechanism, leading to the formation of $CH_x$ species (Fig. 3c) [95].

On pristine and Na-doped $Co_2C(111)$ [52], CO dissociates both directly and via the H-assisted pathway $CO^* + H^* \rightarrow HCO^*$ , which is subsequently deoxygenated to form CH* and O* . Although the presence of Na on the surface increases the energy barriers for both direct and H-assisted C═O dissociation, it also helps to balance the ratio between surface $CH_x$ and CO species and to promote efficient C−C coupling, as discussed later in the text.

### 2.2.2. *Formate/methoxy-mediated pathway*

The formate/methoxy-mediated pathway is also common for higher alcohol synthesis [97,98]. In contrast to the CO pathway, where the C═O bond in $CO_2$ is directly cleaved or cleaved via the formation of COOH* intermediate, the formate/methoxy-mediated pathway takes place on catalysts that are more prone to hydrogenating C atoms, e.g., on Lewis-acid-base pair sites. As shown in Fig. 4a, on single-atom Rh catalysts supported on Ti-doped $CeO_2$ [38], $CO_2$* is adsorbed onto a Lewis acid-based pair with the C atom bound to a Lewis acid site (Rh) and the

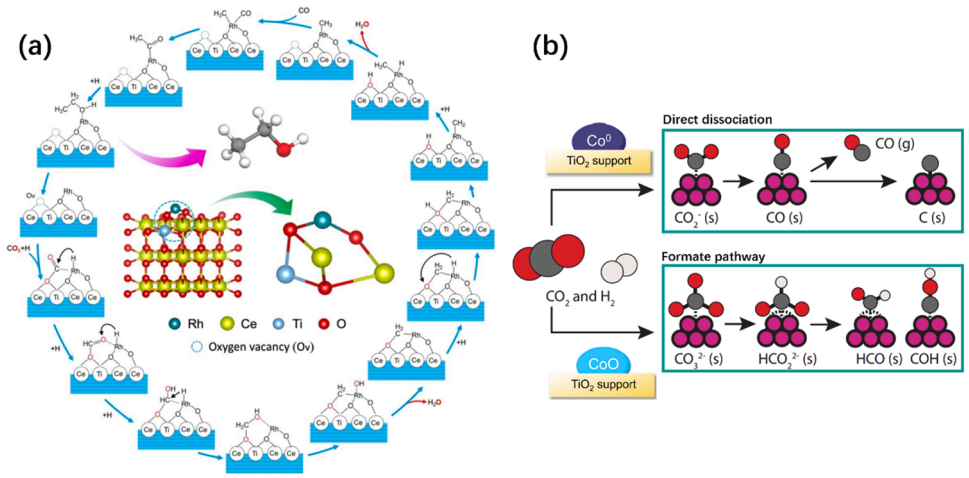


**Fig. 4.** (a) The illustrated catalytic cycle of ethanol formation from $CO_2$ hydrogenation on the $Rh_1/CeTiO_x$ catalyst [38]. (b) Schematic representation of the formate-mediated mechanism, dominant for CoO catalysts, and the direct dissociation mechanism, dominant for metallic Co catalysts [100].
(a) Adapted with permission from Ref. [38]. (b) Adapted with permission from Ref. [100].

O atom bound to the adjacent oxygen vacancy (Ov). The $CO_2$ adsorbed in such a manner exhibits a bent structure, making the carbon center more accessible to hydrogenation into HCOO* . HCOO* is further hydrogenated and deoxygenated to produce $C_1$ building blocks, such as $CH_xOH$* , $CH_x$* , and CO* , which are essential for HA formation (via C–C coupling, as discussed in Section 2.3) [99]. Have et al.[100] found that the CoO catalysts and metallic Co followed different $CO_2$ activation pathways. As shown in Fig. 4b, metallic Co favors the direct C═O dissociation pathway, whereas CoO catalyzes the H-assisted mechanism involving surface formates as intermediates. For the Co-CoO system, the formate-mediated pathway had a higher rate and was more beneficial for producing long-chain hydrocarbons than the direct C═O cleavage pathway. In general, modified Co-based catalysts have been widely used in higher alcohol synthesis and are considered to follow the H-assisted $CO_2$-dissociation mechanism.

### 2.3. C–C coupling

The activation of $CO_2$ (see Section 2.2) can produce a plethora of $C_1$ intermediates (e.g., CO, $CO_3$, $CH_xO$, $CH_x$), which can undergo C–C coupling to form $C_{2+}$ intermediates, leading to the formation of $C_{2+}$ alcohols. As discussed above, the stability of the $C_1$ intermediates, governed by (1) their adsorption strength and (2) the abundance and activity of surface hydrogen, influences the composition of $C_1$ intermediates present on the surface and, ultimately, the mechanism of C–C coupling. The commonly accepted C–C coupling mechanisms include CO insertion, $CO_2$ insertion, $CH_x$–$CH_xO$/$CH_x$ coupling, and $CH_x$–HCOO coupling. Besides higher alcohol synthesis, C–C coupling can also lead to the production of alkanes, olefins, aldehydes, and other byproducts.

#### 2.3.1. CO insertion

The CO insertion mechanism has been widely accepted for higher alcohol synthesis through $CO_2$ hydrogenation on Rh-, Pd-, Pt-, and Cu-based catalysts [39,43,101,102]. It involves the reaction of CO* with alkyl species ($CH_x$*), and the subsequent hydrogenation of the $C_{2+}$ intermediates to $C_{2+}$ alcohols. Higher alcohol synthesis through the CO insertion mechanism requires a balanced amount of both surface $CH_x$* and CO* species, achieved through appropriate rates of dissociative CO activation (alkylation) and nondissociative activation of CO on the catalyst [36,37,50,63,64,103]. Xu et al. [65] demonstrated how to achieve such balance by promoting Cu-Fe-based catalysts with K in K-CuMgZnFe. A moderate amount of K doping (i.e., 4.6 wt%) was found to weaken bridging CO* adsorption while promoting linear CO* adsorption. Moreover, K doping increased the abundance of $CH_x$* , leading to improved formation of $C_2H_5O$* and high selectivity of the catalyst towards HA (Fig. 5). The important role of K promotors was also shown by Liu et al., who studied K-Cu-Fe catalysts supported on amorphous $ZrO_2$ [61]. As shown in Fig. 6a, the surface $Zr^{\delta+}$ sites/oxygen vacancies at the K-$ZrO_2$ interfaces provided empty 4d orbitals to accept lone pair electrons from the C atom of CO and enhanced non-dissociative CO adsorption. In turn, a high surface coverage of CO* facilitated the CO insertion reaction ($CH_x$* + CO* → $CH_x$*–CO) at Cu-$Fe_5C_2$ interfaces and enhanced higher alcohol productivity. The importance of optimizing the concentration of alkali promotors was also noted on Na-$Co_2C$ catalysts for $CO_2$ reduction to ethanol [52]. Whereas low amounts of Na helped balancing the concentration of CO* and $CH_x$* species on the catalyst surface, the addition of more than 5 wt% of Na to the catalyst destabilized $CH_x$* species and undermined the $CO_2$ reduction reaction.

Note that an effective catalyst should not over-hydrogenate CO* and $CH_3$* . For example, Xu et al.[23] used Cs-doping to regulate the hydrogenation activity of the CuFeZn catalyst, which showed enhanced HA yield via CO* insertion into $CH_3$* compared to the Cu-$Fe_7C_3$ interfacial active sites. The feasibility of the CO insertion pathway of $CO_2$ conversion is governed by the adsorption strength of $CH_3$* species, which is influenced by the presence of water and OH* on the catalyst surface. For example, on Pt/$Co_3O_4$ catalyst, He et al.[45] used $D_2O$ and $^{13}CH_3OH$ labeling experiments to demonstrate the ability of water to protonate methanol, which easily dissociated into $CH_3$* , OH* , and H* (or $H_2O$) species. The surface $CH_3$* species would further couple with CO

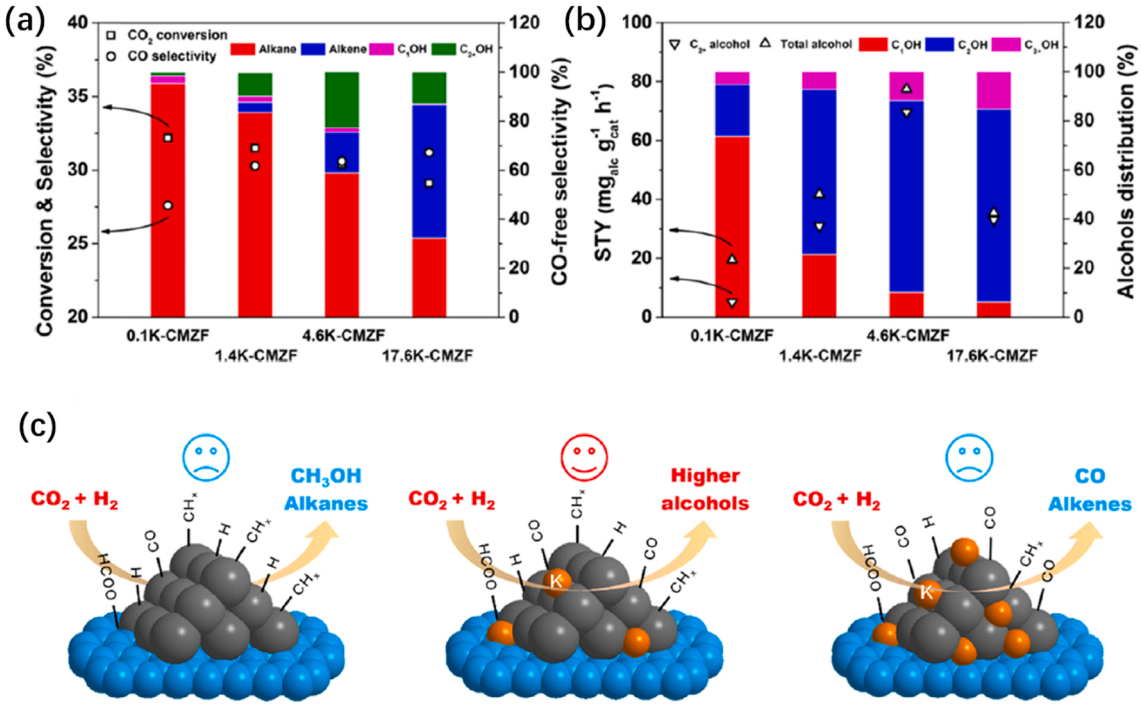


**Fig. 5.** Catalytic performance of $CO_2$ hydrogenation over different xK-CuMgZnFe catalysts. (a) $CO_2$ conversion, CO selectivity, and other product selectivity (mol%, CO-free) toward alkanes, alkenes, methanol, and $C_{2+}$ alcohols and (b) space-time-yield (STY) of $C_{2+}$ alcohols, total alcohols, and alcohol distribution (wt%). (c) Schematic of the tailored product distribution in $CO_2$ hydrogenation over K-CuMgZnFe catalysts with different K contents.
Adapted with permission from Ref. [65].

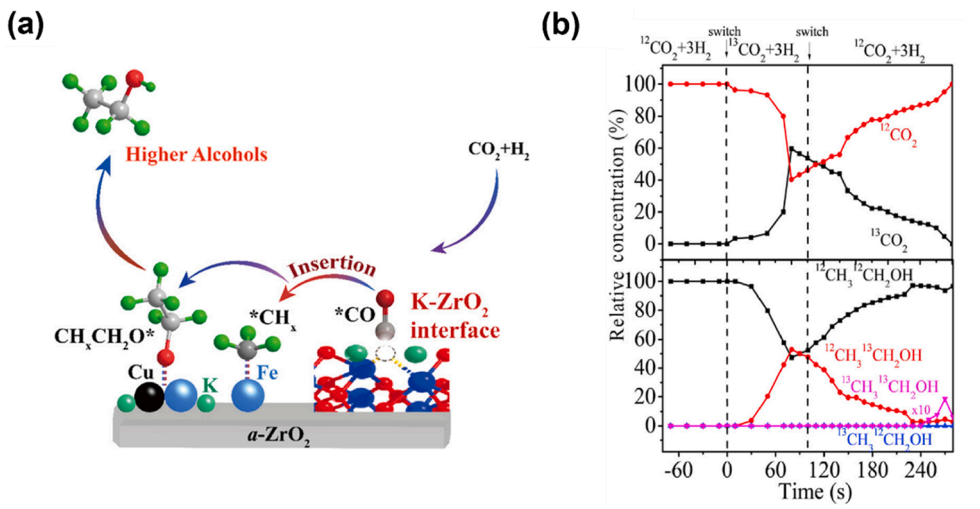


**Fig. 6.** (a) Illustration for the contribution of K-$ZrO_2$ interfaces to higher alcohol synthesis over supported FeCu-based catalysts. [61]. (b) The relative concentrations of $^{13}CO_2$ or $^{12}CO_2$ (monitored at the outlet of the reactor) during switching the reactants between $^{13}CO_2$ + 3 $H_2$ and $^{12}CO_2$ + 3 $H_2$ (top panel); and concentrations of products during $CO_2$ reduction to ethanol over the Cu@Na-Beta zeolite (bottom panel). [66].
(a) Adapted with permission from Ref. [61]. (b) Adapted with permission from Ref. [66].

obtained from the reverse water-gas shift reaction to form $CH_3CO$* , which was subsequently hydrogenated to yield ethanol. The study by Yang et al. also supported the important role of water and surface OH* groups [39] for Rh-based catalysts supported on $TiO_2$ nanorods. Through in situ DRIFTS experiments, they found that the surface coverage of $CH_3$* species correlates linearly with the surface concentration of hydroxyl groups on $TiO_2$. Specifically, it was proposed that the hydroxyl groups could enhance the adsorption of formate intermediates and accelerate the scission of $CH_x$–O to produce $CH_3$* species, thus favoring ethanol formation upon CO insertion.

CO insertion mechanism has also been investigated using density functional simulations, e.g., on ceria-supported catalysts including $Pt_x$/$CeO_x$/$TiO_2$ [104,105], $Rh_1$/$CeTiO_x$ single-atom catalyst (SAC) [38], and $CeO_2$-supported Pd dimers [42]. The excellent catalytic performance of Pt/$CeO_x$/$TiO_2$ was attributed to the unique electronic interaction between ceria and titania. The $Rh_1$/$CeTiO_x$ SAC also exhibited enhanced C–C coupling between CO and $CH_x$ species, resulting in high yield and selectivity towards HA. Moreover, the strong Rh–O bond in $Rh_1$/$CeTiO_x$, resulting from structural reconstruction, contributed to its improved catalytic stability. On $CeO_2$-supported Pd dimers, the DFT calculations suggest $CO_2$ activation by direct C═O cleavage followed by CO insertion to form $CH_3CO$* , which is subsequently hydrogenated to form $CH_3CH_2OH$.

### 2.3.2. *$CO_2$ insertion*

In addition to the CO insertion mechanisms mentioned above, C−C coupling could also proceed through coupling of $CO_2$ with $CH_3$* . In this mechanism, a portion of the adsorbed $CO_2$* is initially hydrogenated to $CH_3$* on the metal sites and then reacts with a neighboring non-hydrogenated $CO_2$* to form $CH_3COO$* [106]. Finally, the $CH_3COO$*- undergoes hydrogenation to form ethanol [107]. Ding et al. [66] deduced the $CO_2$ insertion mechanism from their isotopic-labeling experiments and DFT calculations over a Cu@Na-Beta zeolite catalyst. As shown in Fig. 6b, the synchronous variation of the $^{12}CH_3{}^{13}CH_2OH$ signal with the $^{13}CO_2$ feed indicates that the gaseous $^{13}CO_2$ readily reacts with surface $^{12}CH_3$* to give $^{12}CH_3{}^{13}CH_2OH$ on the step sites of the zeolite-entrapped Cu nanoparticles. Izumi et al. [108] observed the absence of CO* on $RhSe_{10}$/$TiO_2$ during in situ FTIR analysis, while the ethanol production rate appeared to be proportional to the intensities of $CH_3$* and $CH_2$* signals. These observations suggested the $CO_2$ insertion mechanism for ethanol synthesis on $RhSe_{10}$/$TiO_2$, where the $CO_2$ comes from either surface carbonate species or adsorbed $CO_2$* .

### 2.3.3. *$CH_x$–$CH_xO$/$CH_x$ coupling*

The $CH_xO$–$CH_x$ coupling has been widely considered a compelling C–C coupling mechanism with vast supporting observations [95,109, 110]. On catalysts where the adsorption of $CH_x$ and $CH_xO$ species is stronger than that of CO (e.g., on $Cu_6$/$ZnAl_2O_4$) [53], $CH_x$–$CH_xO$ coupling is considered a more likely C–C coupling pathway than CO insertion. Zhang et al. [53] investigated the reaction network of $CO_2$ reduction on $Co_2C$ and CuZnAl multifunctional tandem catalysts. As shown in Fig. 7a, the formation of $C_2H_5O$* (monitored by the symmetrical and asymmetrical vibrations of $CH_3$ ($\delta_s(CH_3)$ and $\delta_{as}(CH_3)$), respectively) is correlated to the consumption of $CH_3O$* , suggesting the coupling of $CH_xO$* with unsaturated C of CHO* or $CH_2O$* species to be a rate-limiting step. While CO insertion is the main C–C coupling mechanism on $Co_2C$ (Fig. 7b), interfacing $Co_2C$ with CuZnAl lowers the energy barrier of $CH_x$–$CH_xO$ coupling and makes it the dominating C–C coupling mechanism instead. Thus, engineering interfacial catalytic sites appears as an accessible and effective approach to tune C–C coupling mechanisms. Wang et al. [60] found using in situ DRIFTS that $CH_x$* –$CH_x$* coupling is prevalent on the surface of Na-Fe@C, which exhibited selectivity towards alkenes and alkanes of 49.5% and 22.8%, respectively. However, after combining Na-Fe@C and K-CuZnAl, the dominating reaction pathway switched to $CH_x$* –$CH_xO$* coupling (Fig. 7c), yielding an enhanced ethanol selectivity of 32.2%. This observation was corroborated by Wang et al., whose calculations showed that the barrier for $CH_x$* –$CH_xO$* coupling is lower than that for CO insertion (i.e., $CH_x$* + CO* → * + $CH_xCO$*) on RhMn supported on the silicate-1 zeolite crystals [111], indicating the important role of $CH_xO$* species for ethanol synthesis.

One source of $CH_xO$ for $CH_x$–$CH_xO$ coupling is the hydrogenation of CO* . It is believed that moderately strong adsorption of CO* is essential for producing a mixture of $CH_x$ and $CH_xO$ building blocks that can be converted to HA, while the weak binding of CO* on the catalyst surface leads to CO production [70]. However, extremely strong adsorption of CO would result in full CO hydrogenation and high selectivity towards methane and/or methanol.

$CH_x$–$CH_xO$ coupling has also been studied computationally by many researchers. For instance, Zhang et al. conducted a DFT investigation to outline a reaction network, elucidating the carbon chain growth and $C_2$ oxygenate formation [112–114]. Their findings highlight the significance of various surface sites on Cu(100) and stepped Cu(211) surfaces in various steps of ethanol formation via the CHO insertion into $CH_3$. For example, the hollow sites favor CO hydrogenation, whereas the

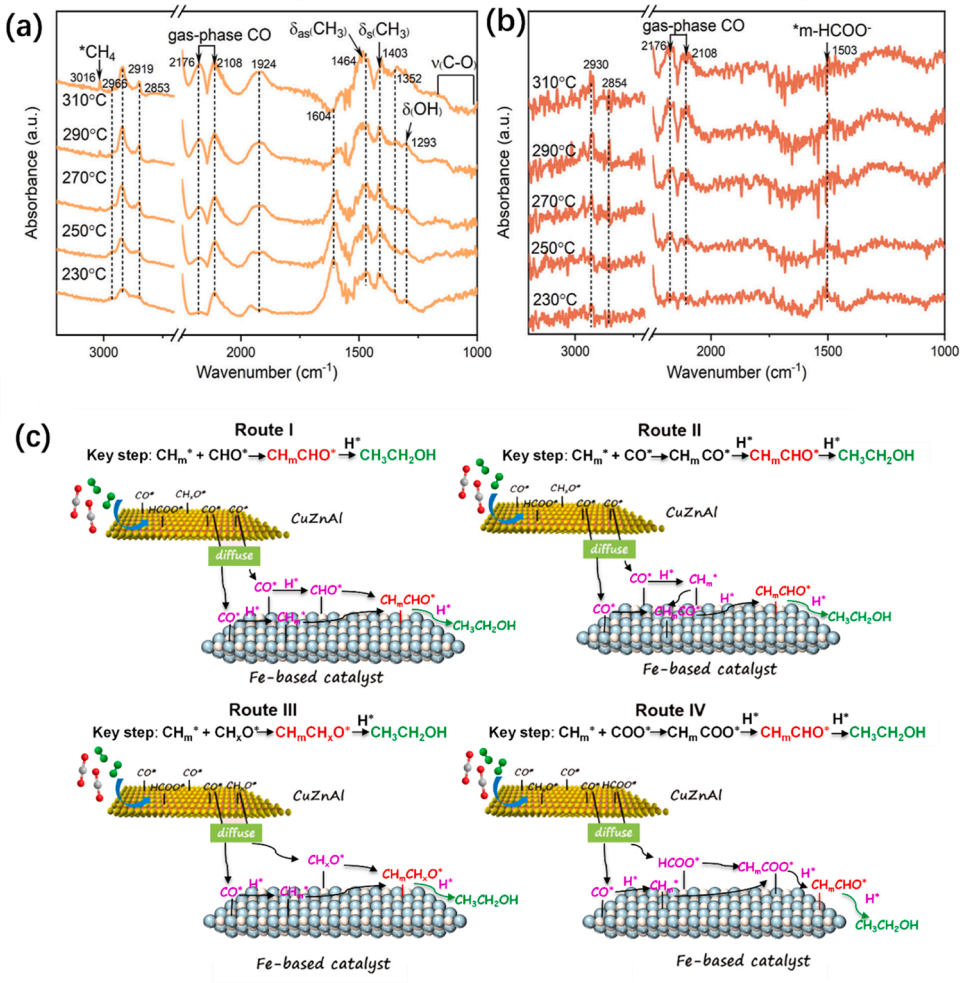


**Fig. 7.** *In situ* DRIFTS spectra taken during $CO_2$ hydrogenation over (a) CuZnAl and (b) $Co_2C$ surface in $Co_2C$||CuZnAl at different temperatures. [53]. (c) Reaction network for ethanol synthesis from $CO_2$ hydrogenation via the Na-Fe@C/K-CuZnAl multifunctional catalyst. [60].
(a), (b) Adapted with permission from Ref. [53]. (c) Adapted with permission from Ref. [60].

formation of $CH_3$ takes place at the bridge and top sites. In turn, on Cu (211), the step edge sites are actively involved in key reactions, such as the insertion of CHO* into $CH_3$* to form $CH_3CHO$* . Furthermore, the introduction of Mn [115] promoters onto Cu(211) enhances catalyst activity for CHO insertion into $CH_3$. Additionally, Rh-decorated Cu catalyst has been shown to modulate the energetics of key elementary steps, such as $CH_3$ formation and CO insertion, while effectively suppressing methanol formation to achieve high productivity and selectivity for ethanol [115,116]. Notably, two key variables strongly influence the productivity and selectivity of $C_2H_5OH$: the rate of formation of $CH_3$ and the rate of formation of CHOH.

Wang et al. [117] examined ethanol, methanol, and methane synthesis from syngas using Fe-based catalysts. The optimal pathway for ethanol formation involves CO dissociation and hydrogenation to $CH_3$* , followed by CHO* insertion into $CH_3$* to form $CH_3CHO$* , which is then hydrogenated to ethanol. The selectivity for ethanol is influenced by the concentration of methyl species and their coupling with CHO* groups. Among the studied catalysts, Cu-Fe exhibits the highest ethanol selectivity, followed by Pd-Fe, while $Cu_9$/Fe(100) and $Fe_9$/Fe(100) show the lowest selectivity. The Fe sites on the catalyst favor the formation of $CH_x$* species, while the presence of Cu and Pd sites is crucial for providing undissociated CO* /CHO* species. Catalysts containing Cu/Fe and Pd/Fe provide dual active sites that work synergistically to facilitate chain propagation. This synergy enables the insertion of CO* /CHO* groups into $CH_x$* species, leading to the generation of surface $C_2$ oxygenates.

Notably, $CH_x$–$CH_xO$ coupling also enables the formation of $C_{3+}$ alcohols. Irshad et al. [59] demonstrated the direct and selective production of $C_{3+}$ alcohols that are rich in *n*-butanol via $CO_2$ hydrogenation over a bimetallic Co-Cu tandem catalyst, deviating from the Anderson–Schulz–Flory (ASF) distribution. In the proposed mechanism, $CH_3$* interacts with CO* to produce a $C_{2+}$ oxygenate intermediate, further hydrogenated to acetaldehyde. Subsequently, the acetaldehyde intermediate is re-activated on the Cu surface to a mixture of $CH_3CHOH$* + $CH_2CHO$* . The facilitated C–O bond dissociation of $CH_3CHOH$* over the Co site produces $CH_3CH$* , which subsequently couples with $CH_2CHO$* to form $C_4$ oxygenates as precursors to the formation of *n*-butanol. The termination reaction (to form $CH_4$) simultaneously occurs over the Co surface and competes for $CH_x$* with CO* insertion. Nevertheless, the selectivity towards the termination reaction could be controlled by varying the Co content.

Therefore, designing higher alcohol synthesis catalysts containing active sites that are capable of adsorbing CO* at appropriate strength and stabilizing oxygenated species is essential for achieving a balanced surface coverage of $CH_x$* and $CH_xO$* species for high HA selectivity via the $CH_x$–$CH_xO$ coupling mechanism.

### 2.3.4. $CH_x$ –HCOO coupling

The coupling of HCOO* to $CH_x$* leads to the formation of acetate, which can be further hydrogenated to ethanol. Wang et al. [54] proposed

the $CH_x$–HCOO coupling mechanism on a Co-based catalyst ($CoAlO_x$). Through in situ FTIR and $^1H$ MAS NMR spectroscopy, the emergence of $CH_x$* and HCOO* intermediates was observed upon the hydrogenation of a carbonated catalyst surface covered by $CO_2$*, $CO_3^{2-}$, and $HCO_3$* . Subsequently, $CH_x$* coupled with HCOO* to form acetate, which was a key intermediate for ethanol synthesis. In another study, Wang et al. explored the surface concentrations of various $C_1$ intermediates (HCOO*, $CH_x$*) and coupling between them through a mathematical model and accordingly developed an efficient Co-Ni catalyst, $Co_{0.52}Ni_{0.48}AlO_x$, for ethanol production [55]. As shown in Fig. 8a, FTIR experiments found that the unbalanced concentrations of key $C_1$ intermediates (viz. HCOO* and $CH_x$*) hindered the $C_2$ intermediates production. In comparison, $Co_{0.52}Ni_{0.48}AlO_x$ could enhance the production of $CH_x$* species and modulate the population of surface intermediates. The obtained catalyst exhibited high ethanol productivity via $CH_x$–HCOO coupling with an ethanol yield of 1.3 mmol $g^{-1}$ $h^{-1}$ and an ethanol selectivity of 85.7% at 200 ℃ in an initial pressure of 4.0 MPa ($H_2/CO_2$ = 3:1). Although Ni is an ineffective catalyst for ethanol synthesis, alloying it with Co enhanced its hydrogenation ability for the fast production and stabilization of $CH_x$* , leading to enhanced ethanol selectivity.

### 2.3.5. Other C–C coupling mechanisms

Besides CO insertion, $CO_2$ insertion, $CH_x$–$CH_xO$ coupling, and $CH_x$–HCOO coupling, other C–C coupling mechanisms have also been proposed in the literature. For example, An et al.[62] found that C–C coupling takes place between methanol and formyl species over diatomic $Cu_2^I$ centers (Fig. 8b), promoted by alkali metals (e.g., Cs or Li) on $Zr_{12}$-bpdC-Cu catalysts. The key role of formyl intermediates was confirmed by a control experiment, in which the hydrogenation of formaldehyde (HCHO) also produced ethanol. In addition, EtOH selectivity was found to improve with increased methanol concentration in the system. The methanol-formyl coupling mechanism was further confirmed by $^{13}C$ and deuterium labeling experiments, suggesting the following reaction pathway: $^{13}CH_3OH + CO_2 + H_2 \rightarrow CH_3CH_2OH + {}^{13}CH_3CH_2OH$ and $CD_3OH + CO_2 + H_2 \rightarrow CH_3CH_2OH + CD_3CH_2OH$.

A related C–C coupling mechanism between $CH_3$* species and $CH_2O$ was proposed for $Pt/CeO_x/TiO_2$ catalysts for $CO_2$ reduction to methanol and ethanol [104]. The kinetics of these reactions were found to be strongly affected by water molecules, which facilitated $CO_2$ activation and deoxygenation of $CH_3O$* intermediates into $CH_3$* species involved in the C–C coupling step.

C–C coupling between $CH_3$* and $CH_2$* was proposed on the Cu active sites in PCN-224-Cu, composed of $Zr_6$ cluster and TCPP-Cu unit (Fig. 8c). The $Zr_6$ cluster was proposed to be in charge of C═O cleavage steps (including $CO_2 \rightarrow O^* + CO^*$ and $CH_3OH \rightarrow CH_3^* + OH^* \rightarrow CH_2^* + H_2O$), while the TCPP-Cu unit was responsible for the assembly of intermediates generated on the $Zr_6$ cluster. Based on DFT calculations, the first step in the reaction mechanism on this catalyst was proposed to be $CO_2$ dissociation to CO* on the $Zr_6$ cluster, followed by methanol formation on TCPP-Cu through rapid CO hydrogenation. During the conversion of methanol to ethanol, the $Zr_6$ cluster was speculated to catalyze the decomposition of methanol to $CH_3$* and OH* and the further decomposition of $CH_3$* to $CH_2$* . The decomposition of $CH_3OH$, formation of $CH_3$* and $CH_2$* intermediates, and their coupling were verified by in situ DRIFTS [67].

Wang [118] proposed a CHO−CHO coupling mechanism during $CO_2$ hydrogenation to HA over a model Cu/Cs/ZnO $(000\bar{1})$ catalyst structure based on DFT and kinetic Monte Carlo (KMC) simulations. The KMC showed that HCOOH* was the active intermediate originating from the formate pathway on both Cu/ZnO $(000\bar{1})$ and Cu/Cs/ZnO $(000\bar{1})$. Without Cs, HCOOH* was mostly hydrogenated to $H_2COOH$* and decomposed to $CH_2O$* on Cu/ZnO $(000\bar{1})$; in turn, the $CH_2O$* was further hydrogenated to $CH_3OH$. The higher selectivity to $CH_3OH$ on Cu/ZnO $(000\bar{1})$ was attributed to the higher rate of hydrogenation of CHO* to $CH_2O$* rather than accelerated C−C coupling between CHO* species. On Cu/Cs/ZnO $(000\bar{1})$, a synergy among Cs, Cu, and ZnO promoted the interaction with $CO_2$ and enhanced the binding of CHO* , which was identified as the key precursor to initiate C–C coupling and form OHCCHO* . OHCCHO* is eventually transformed to ethanol via successive hydrogenation: $OHCCH_2O^* \rightarrow OHCCH_2OH^* \rightarrow OHCCH_2^* \rightarrow OH_2CCH_2^* \rightarrow OH_2CCH_3^*$ . This study shows the importance of fine-tuning the adsorption strength of CHO* to the catalyst surface for the effective C–C coupling to yield higher alcohols.

The discussion above summarizes the possible C–C coupling mechanisms for synthesizing HA via catalytic $CO_2$ hydrogenation. Given the diverse $C_1$ building blocks that could be present on the catalyst surface and capable of C–C coupling reactions, one could foresee challenges in discriminating the various reaction mechanisms. To this end, combining experimental and computational analyses is essential for establishing the structure-function relationships toward the rational design of catalysts for $CO_2$ reduction to higher alcohols.

## 3. Outlook: Rational catalyst design aided by mechanistic insights

### 3.1. Bottlenecks in the rational catalyst design and scaling up

The complex reaction network with a wide product distribution is a major challenge to the rational and effective design of catalysts with

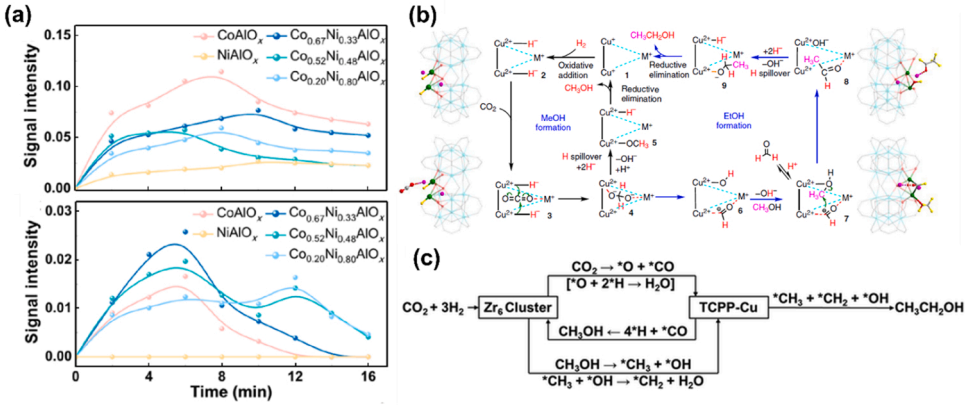


**Fig. 8.** (a) IR peak intensity of HCOO* (top panel) and $CH_x$* (bottom panel) intermediates on the $CO_2$ pretreated $Co_{0.52}Ni_{0.48}AlO_x$ catalyst. [55] (b) Formyl-methanol coupling mechanism for $CO_2$ hydrogenation to ethanol over $Zr_{12}$-bpdC-Cu catalysts. [62]. (c) The derived mechanism of $CO_2$ hydrogenation to ethanol over PCN-224-Cu. [67].
(a) Adapted with permission from Ref. [55]. (b) Adapted with permission from Ref. [62]. (c) Adapted with permission from Ref. [67].

high efficiency in the $CO_2$-to-HA process. In this review, we emphasize that the design of active and selective $CO_2$-to-HA catalysts should address three key sub-processes, namely, $H_2$ activation and spillover, $CO_2$ adsorption and activation, and C−C coupling. Extensive studies have been performed in the past decades to understand how catalytic structures affect the stabilities of key reaction intermediates, which dictate the rate-limiting steps, the reaction pathways, and ultimately, the catalytic performance through structure-activity relationships. Although significant advancements have been achieved in the mechanistic investigation of $CO_2$-to-HA catalysts, there is still a need to address several critical issues in this area, as detailed below.

Developing robust synthetic approaches to tune catalyst activity and selectivity remains challenging. Trade-offs between activity and selectivity are often reported, complicating the search for catalysts that excel in both aspects. For instance, strong $H_2$ activation ability often corresponds to high Fischer-Tropsch activity [119], which means reduced selectivity towards HA. Future experimental studies, therefore, should focus on elucidating the evolution of the catalytically active sites under working conditions and developing performance enhancement strategies as outlined below.

Firstly, the reactor design and the reaction conditions need to be optimized to ensure that the driving forces for the reaction are in optimal regimes [120]. Optimizing reactors and reaction conditions is particularly important since the synthesis of higher alcohols through $CO_2$ hydrogenation results in a mixture of alcohols that requires separation for downstream processing. The product distribution in HA synthesis is heavily influenced by both the catalyst composition and reaction conditions. For example, Cu catalysts enable the synthesis of methanol at low $CO_2$ pressure or $C_{3+}$ alcohols at higher reaction pressures (> 4 MPa), whereas ethanol is hardly produced on Cu catalysts [59]. The separation process of various HAs is energy-intensive, making it imperative to optimize the selectivity of a specific alcohol within the HA category.

Secondly, the continuous improvement of catalyst performance remains critical to advancing this process toward commercialization. As systematically discussed in this review, the activity and selectivity of the catalyst towards desired products can be enhanced by engineering defect sites [121], acid-base pairs [38], mixed oxides [44,55,86], or bimetallic alloys [70,80,93,95]. Furthermore, the selectivity of the reaction can be steered without sacrificing the rate of $CO_2$ conversion by designing catalysts possessing multiple functionalities (e.g., $CO_2$ hydrogenation catalysts and C–C coupling catalysts) or using tandem catalytic beds. In fact, using multifunctional catalysts is a common strategy for complex chemical transformations. Multifunctionality is often realized by combining two or more well-established catalytic processes, such as (1) combining the reverse water-gas shift reaction with the Fischer-Tropsch synthesis or (2) combining methanol synthesis with methanol-to-hydrocarbon reactions [122]. In multifunctional and/or cascade catalysis systems, limitations, such as scaling relationships between binding energies of various adsorbates, may be bypassed by using catalysts combining diverse active sites [123] or catalysts whose specific active sites can catalyze several elementary reactions. Indeed, many studies discussed in this review have explored multifunctional catalysts and, or multifunctional sites. For example, a potassium-doped methanol synthesis CuZnAl catalyst was combined with a Na-Fe@C catalyst promoting both $CH_2$–CHO and $CH_2$–CO coupling reactions [60]. Bifunctional $Ir_1$-$In_2O_3$ sites were found to both catalyze the abstraction of O from $CO_2$ and the subsequent coupling of CO* with methoxy species [48]. DFT calculations rationalized the multifunctionality of Cu-Cs-ZnO sites, which can catalyze $CO_2$ activation, HCOOH decomposition to CHO, and CHO–CHO coupling [118]. Similarly, dual Pd-Pd [124] and $Co_1$ @Cu(211) sites [59] have been suggested to be bifunctional towards C–O cleavages and C–C coupling. Nevertheless, the design of multifunctional catalysts is more challenging than that of monofunctional catalysts since it requires precise control of the catalytic activity to balance the migration of the various reaction intermediates between different catalyst components.

Thirdly, although past catalyst characterization studies (e.g., by in situ DRIFTS) have shed light on the mechanism for $CO_2$ activation and C–C coupling, there are insufficient comprehensive studies utilizing in situ and operando characterization techniques to investigate the structure of the active sites at practically relevant operating conditions. Similarly, computational studies (e.g., DFT calculations) are often performed assuming idealized operating temperatures and pressures (e.g., at 0 K in vacuum). Such temperature and pressure conditions significantly differ from those in industrial processes and prevent the atomic-level understanding of the structures of the working catalysts, which is essential information for rational catalyst design. Therefore, future experimental efforts should prioritize the investigation of the dynamic changes of the active sites and the interactions between the species on active centers (e.g., during C–C coupling) using in situ and operando diffraction spectroscopic techniques under conditions that are relevant for commercial deployment of the $CO_2$-to-HA process. Additionally, efforts should be devoted to developing computational methods capable of modeling the catalytic process in more realistic conditions, incorporating kinetic Monte Carlo and microkinetic simulations in conjunction with DFT calculations to accurately capture the complexity of the $CO_2$ hydrogenation process at elevated pressures and temperatures. The combination of operando experimental characterization with realistic DFT simulations will enhance the understanding of the catalytic activity at the atomic scale and facilitate the rational design of more efficient and selective catalysts for $CO_2$ hydrogenation.

Fourthly, lab-based studies of $CO_2$ hydrogenation catalysts mostly focused on exploring structure-function relationships. Therefore, catalysts are often formulated prioritizing control of particle sizes, distinct active sites, and compositional simplicity (for the ease of modeling and structural characterizations). These considerations could make the catalysts studied in the lab differ significantly from those used in the industry. For example, the catalyst ($Cu/ZnO/Al_2O_3$) for industrial methanol synthesis typically contains around 70 wt% Cu. It would be challenging for experimental studies to precisely control the particle size of Cu or the densities of Cu/ZnO interfaces with such high Cu contents.

Furthermore, lab-based catalysis research uses rather idealized testing conditions, e.g., stable gas flows, minimized heat effects, small catalyst particle sizes, high-purity inlet gases, and moderate operating pressures. As the catalyst research moves from lab scale to pilot and industrial scales, new challenges could emerge during large-scale operations and must be addressed prior to successful commercialization. For instance, understanding and optimizing heat dissipation in the catalytic material will be essential for safe and efficient operation. To this end, utilizing computer-aided design tools such as 3D printing and computational fluid dynamics (CFD) modeling can accelerate the optimization of reactor design and associated process parameters. In industrial settings, catalysts may encounter contaminants or impurities that could poison or deactivate the catalysts, reducing their activity and selectivity over time. Therefore, developing catalytic materials that have excellent stability and resistance in the presence of impurities and contaminants is essential. Last but not least, ensuring that the catalysts are low-cost, environmentally friendly, easy to separate, and easy to recycle should also be prioritized during their development.

### 3.2. Computational design of catalysts

Computational studies are expected to continue playing a major role in the fundamental studies and development of catalysts for $CO_2$ reduction to higher alcohols. For example, DFT modeling is one of the best tools for the investigation of $CO_2$ reduction mechanisms, given its intrinsic atomic resolution and the ability to characterize even unstable and short-lived reaction intermediates, which can participate in reaction steps that determine catalyst activity and selectivity. Mechanistic understanding that stems from DFT modeling is the foundation of microkinetic modeling that, in turn, can facilitate the design of novel catalysts

and the selection of optimal operating conditions. However, comprehensive DFT studies of higher alcohol synthesis mechanisms are expected to be computationally expensive. For example, one could expect the complexity of higher alcohol synthesis from $CO_2$ to exceed that from syngas, which includes almost one hundred tentative intermediates and almost two hundred transition states [125]. We believe that the exponential growth of computational power will soon allow detailed and comprehensive modeling of the wide reaction network for $CO_2$ reduction to higher alcohols, including all possible side reactions and byproducts, such that the critical steps in the reaction mechanism on any catalyst surface could be identified to enable the rational catalyst design. On the other hand, research efforts should also focus on developing methods that reduce the inherent complexity of the problem, e.g., using machine learning (ML) and deep learning (DL) techniques. In fact, ML and DL techniques have been actively employed in the area of CO and $CO_2$ hydrogenation processes for the following:

1) Estimating activity (or virtual screening) of catalytic systems based on experimental data [126,127]
2) Analyzing key catalyst features based on experimental data [126–128]
3) Addressing the complexity of catalytic reaction networks [125,129]
4) Using ML potentials and surrogate models to perform CPU-efficient modeling of catalytic processes and catalytic materials [130–134].

Moreover, the generative DL and classic ML methods can be used to discover novel $CO_2$ reduction catalysts. However, the efficiency of such methods strongly depends on the quality of the training data [127], which have become increasingly more available through various materials databases [135–140], some of which also contain the materials' catalytic properties [141,142]. In particular, the Open Catalyst database [141] contains DFT-generated thermodynamic data on chemical reactions related to CO and $CO_2$ hydrogenation processes, which can facilitate DL-based prediction of highly active catalysts using generative artificial intelligence in the near future. It should be noted that DL- and ML-driven prediction of candidate catalysts requires precise mapping of the catalytic activity to material descriptors, such as adsorption energies of reacting species and the d-band centers of transition metals, both of which often exhibit Sabatier volcano relation with the activity of the catalyst [143,144]. Using the established volcano relationship, one can rapidly evaluate descriptors for thousands of candidate materials using ML/DL models, whose accuracy can closely match that of density functional calculations [145,146]. Such an approach has been used to predict homogeneous and electrochemical catalysts for $CO_2$ reduction into various products [144,147], as well as for virtual screening of catalysts or active center structures for heterogeneous CO and $CO_2$ hydrogenation [148–151]. One could expect approaches combining ML methods with density functional calculations to yield fruitful results for the discovery of new catalysts for $CO_2$ reduction to higher alcohols. To this end, a deeper understanding of the complex reaction network is the prerequisite for developing an efficient high-throughput screening method.

Although ML-assisted methodologies have been developed and used successfully in heterogeneous catalyst research in general and $CO_2$ hydrogenation research in particular, no ML-assisted studies of thermocatalytic $CO_2$ hydrogenation to HA have been reported to the best of our knowledge. Nevertheless, numerous ML-assisted studies have been conducted on $CO_2$ reduction into other products, such as methanol or formic acid, as well as on higher alcohol synthesis from syngas. Owing to the complexity of the reaction pathways involved in $CO_2$-to-HA and the efficiency of ML methods in addressing such complexity through computationally screening catalysts/active sites, numerous ML-assisted studies of catalysts for $CO_2$ reduction to HA are expected to emerge soon.

## 4. Conclusions

The intensity of research on $CO_2$ reduction to HA has significantly increased in recent years in an attempt to develop economically attractive chemical processes using $CO_2$ as a feedstock. Although various catalysts have been proposed for this reaction, their future development is hindered by the limited understanding of higher alcohol synthesis mechanisms. The reaction network for $CO_2$ reduction to HAs contains a great number of elementary steps, whose rates and importance for the reaction kinetics may vary significantly on different types of catalysts. For example, various materials can catalyze C–C coupling between CO, $CO_2$, $CH_x$, $CH_xO$, or HCOO reaction intermediates during $CO_2$ reduction reactions. On the one hand, such complexity in the higher alcohol synthesis mechanism implies that findings from one group of catalysts may not necessarily be generalizable to other catalytic systems for higher alcohol synthesis. On the other hand, such a complex reaction mechanism also opens numerous opportunities for catalyst development by preventing any single elementary step from being the kinetic bottleneck.

Previous research also suggested various strategies to improve the activity of $CO_2$ reduction catalysts. For example, the direct dissociation of $CO_2$ to CO and O can be efficiently catalyzed by vacancy-rich oxides. The kinetics of H-assisted $CO_2$ activation and the subsequent C–C coupling are also governed by the stability of HCOO or $CH_xO$ intermediates on the catalyst surface. Another necessary reactant in higher alcohol synthesis is molecular hydrogen, whose slow activation limits the $CO_2$ reduction rate on oxide catalysts. In general, hydrogen activation may be accelerated by promoting the catalysts with transition metals if one could achieve efficient spillover of hydrogen atoms to the active sites for higher alcohol synthesis.

Improving the selectivity of the $CO_2$ reduction catalysts towards HA production is less straightforward. Many studies discuss how various promotors can tune and balance the concentrations of reaction intermediates involved in C–C coupling on the catalyst surface to facilitate the production of $C_{2+}$ compounds instead of less valuable $C_1$ species. Controlling the abundance and activity of surface H is also extremely important for higher alcohol synthesis to prevent the over-hydrogenation of surface intermediates, e.g., into alkanes.

We expect rapid development in the $CO_2$ to HAs technology in the coming years to originate from the following research directions. First, the development of a deeper understanding of the reaction mechanism is necessary for elaborating more powerful strategies for the design of advanced higher alcohol synthesis catalysts. Second, *in situ* and *operando* characterization of higher alcohol synthesis catalysts and their basic building blocks is necessary to reveal the transformations of active catalytic phases under harsh industrial conditions of $CO_2$ reduction reactions. Finally, applying generative machine learning techniques to catalyst discovery can yield fruitful results when combined with high-throughput experimental or comprehensive computational studies. We believe these advances will soon result in the development of advanced higher alcohol synthesis catalysts for the urgently needed $CO_2$ conversion technologies that are sufficiently economically attractive for widespread deployment.

## CRediT authorship contribution statement

**Yao Sheng:** Conceptualization, Investigation, Writing – Original Draft; **Mikhail V. Polynski, Mathan K. Eswaran, Bikun Zhang:** Investigation, Writing – Original Draft; **Alvin M. H. Lim:** Investigation; **Lili Zhang, Jianwen Jiang:** Writing – Review & Editing, Funding Acquisition; **Wen Liu, Sergey M. Kozlov:** Writing – Original Draft, Writing – Review & Editing, Funding Acquisition, Supervision.

## Declaration of Competing Interest

The authors declare the following financial interests/personal relationships which may be considered as potential competing interests:

Sergey M. Kozlov reports financial support was provided by Agency for Science Technology and Research Research Support Centre.

## Data Availability

No data was used for the research described in the article.

## Acknowledgements

This work is supported by Agency for Science, Technology and Research (A*STAR) through Low Carbon Energy Research Finding Initiative (LCERFI01–0033 | U2102d2006). Y.S and W.L extend their acknowledgement of financial support by National Research Foundation of Singapore under its Campus for Research Enterprise and Technological Excellence (CREATE) programme.

## References

[1] U.J. Etim, Y. Song, Z. Zhong, Improving the Cu/ZnO-based catalysts for carbon dioxide hydrogenation to methanol, and the use of methanol as a renewable energy storage media, Front. Energy Res. 8 (2020) 1–26, https://doi.org/10.3389/fenrg.2020.545431.

[2] X. Xiaoding, J.A. Moulijn, Mitigation of $CO_2$ by chemical conversion: plausible chemical reactions and promising products, Energy Fuels 10 (1996) 305–325, https://doi.org/10.1021/ef9501511.

[3] J. Podder, B.R. Patra, F. Pattnaik, S. Nanda, A.K. Dalai, A review of carbon capture and valorization technologies, Energies 16 (2023) 2589, https://doi.org/10.3390/en16062589.

[4] L. Fu, Z. Ren, W. Si, Q. Ma, W. Huang, K. Liao, Z. Huang, Y. Wang, J. Li, P. Xu, Research progress on $CO_2$ capture and utilization technology, J. $CO_2$ Util. 66 (2022), 102260, https://doi.org/10.1016/j.jcou.2022.102260.

[5] M. Takht Ravanchi, S. Sahebdelfar, Catalytic conversions of $CO_2$ to help mitigate climate change: Recent process developments, Process Saf. Environ. Prot. 145 (2021) 172–194, https://doi.org/10.1016/j.psep.2020.08.003.

[6] F. Nocito, A. Dibenedetto, Atmospheric $CO_2$ mitigation technologies: carbon capture utilization and storage, Curr. Opin. Green. Sustain. Chem. 21 (2020) 34–43, https://doi.org/10.1016/j.cogsc.2019.10.002.

[7] T. Len, R. Luque, Addressing the $CO_2$ challenge through thermocatalytic hydrogenation to carbon monoxide, methanol and methane, Green. Chem. 25 (2023) 490–521, https://doi.org/10.1039/d2gc02900f.

[8] Y. Lei, Z. Wang, A. Bao, X. Tang, X. Huang, H. Yi, S. Zhao, T. Sun, J. Wang, F. Gao, Recent advances on electrocatalytic $CO_2$ reduction to resources: Target products, reaction pathways and typical catalysts, Chem. Eng. J. 453 (2023), 139663, https://doi.org/10.1016/j.cej.2022.139663.

[9] Y. Wang, E. Chen, J. Tang, Insight on reaction pathways of photocatalytic $CO_2$ conversion, ACS Catal. 12 (2022) 7300–7316, https://doi.org/10.1021/acscatal.2c01012.

[10] W.K. Fan, M. Tahir, Recent developments in photothermal reactors with understanding on the role of light/heat for $CO_2$ hydrogenation to fuels: A review, Chem. Eng. J. 427 (2022), 131617, https://doi.org/10.1016/j.cej.2021.131617.

[11] M. Hanifa, R. Agarwal, U. Sharma, P.C. Thapliyal, L.P. Singh, A review on $CO_2$ capture and sequestration in the construction industry: Emerging approaches and commercialised technologies, J. $CO_2$ Util. 67 (2023), 102292, https://doi.org/10.1016/j.jcou.2022.102292.

[12] L. Jiang, W. Liu, R.Q. Wang, A. Gonzalez-Diaz, M.F. Rojas-Michaga, S. Michailos, M. Pourkashanian, X.J. Zhang, C. Font-Palma, Sorption direct air capture with $CO_2$ utilization, Prog. Energy Combust. Sci. 95 (2023), 101069, https://doi.org/10.1016/j.pecs.2022.101069.

[13] S.M. Jarvis, S. Samsatli, Technologies and infrastructures underpinning future $CO_2$ value chains: A comprehensive review and comparative analysis, Renew. Sust. Energy Rev. 85 (2018) 46–68, https://doi.org/10.1016/j.rser.2018.01.007.

[14] R. Chauvy, G. De Weireld, $CO_2$ utilization technologies in Europe: A short review, Energy Technol. 8 (2020) 1–17, https://doi.org/10.1002/ente.202000627.

[15] S.A. Shirazi, B. Abdollahipoor, B. Windom, K.F. Reardon, T.D. Foust, Effects of blending $C_3$-$C_4$ alcohols on motor gasoline properties and performance of spark ignition engines: A review, Fuel Process. Technol. 197 (2020), 106194, https://doi.org/10.1016/j.fuproc.2019.106194.

[16] S.M.N. Rahaju, I. Veza, N. Tamaldin, A. Sule, A.C. Opia, M.B. Abdulrahman, D. W. Djamari, Acetone-butanol-ethanol as the next green biofuel – A review, Automot. Exp. 5 (2022) 251–260, https://doi.org/10.31603/ae.6335.

[17] F. Zeng, X. Xi, H. Cao, Y. Pei, H.J. Heeres, R. Palkovits, Synthesis of mixed alcohols with enhanced $C_{3+}$ alcohol production by CO hydrogenation over potassium promoted molybdenum sulfide, Appl. Catal., B 246 (2019) 232–241, https://doi.org/10.1016/j.apcatb.2019.01.063.

[18] X. Gao, T. Zhang, Y. Wu, G. Yang, M. Tan, X. Li, H. Xie, J. Pan, Y. Tan, Isobutanol synthesis from syngas on Zn-Cr based catalysts: New insights into the effect of morphology and facet of ZnO nanocrystal, Fuel 217 (2018) 21–30, https://doi.org/10.1016/j.fuel.2017.12.065.

[19] C.H. Vo, C. Mondelli, H. Hamedi, J. Pérez-Ramírez, S. Farooq, I.A. Karimi, Sustainability assessment of thermocatalytic conversion of $CO_2$ to transportation fuels, methanol, and 1-propanol, ACS Sustain. Chem. Eng. 9 (2021) 10591–10600, https://doi.org/10.1021/acssuschemeng.1c02805.

[20] C.H. Vo, J. Pérez-Ramírez, S. Farooq, I.A. Karimi, Prospects of producing higher alcohols from carbon dioxide: A process system engineering perspective, ACS Sustain. Chem. Eng. 10 (2022) 11875–11884, https://doi.org/10.1021/acssuschemeng.2c02810.

[21] B. Sharma, C. Larroche, C.G. Dussap, Comprehensive assessment of 2G bioethanol production, Bioresour. Technol. 313 (2020), 123630, https://doi.org/10.1016/j.biortech.2020.123630.

[22] K. Zhang, F. Zhang, Y.R. Wu, Emerging technologies for conversion of sustainable algal biomass into value-added products: A state-of-the-art review, Sci. Total Environ. 784 (2021), 147024, https://doi.org/10.1016/j.scitotenv.2021.147024.

[23] D. Xu, M. Ding, X. Hong, G. Liu, S.C.E. Tsang, Selective $C_{2+}$ alcohol synthesis from direct $CO_2$ hydrogenation over a Cs-promoted Cu-Fe-Zn catalyst, ACS Catal. 10 (2020) 5250–5260, https://doi.org/10.1021/acscatal.0c01184.

[24] M. Zhang, H. Gong, Y. Yu, DFT study of key elementary steps for $C_{2+}$ alcohol synthesis on bimetallic sites of Cu-Co shell-core structure from syngas, Mol. Catal. 443 (2017) 165–174, https://doi.org/10.1016/j.mcat.2017.10.009.

[25] S. He, W. Wang, Z. Shen, G. Li, J. Kang, Z. Liu, G.C. Wang, Q. Zhang, Y. Wang, Carbon nanotube-supported bimetallic Cu-Fe catalysts for syngas conversion to higher alcohols, Mol. Catal. 479 (2019), 110610, https://doi.org/10.1016/j.mcat.2019.110610.

[26] R. Wei, Z. Gao, W. Huang, The structure-activity relationship of AlOOH for CO hydrogenation, Mol. Catal. 548 (2023), 113457, https://doi.org/10.1016/j.mcat.2023.113457.

[27] J. Wang, G. Li, Z. Li, C. Tang, Z. Feng, H. An, H. Liu, T. Liu, C. Li, A highly selective and stable ZnO-$ZrO_2$ solid solution catalyst for $CO_2$ hydrogenation to methanol, Sci. Adv. 3 (2017), e1701290, https://doi.org/10.1126/sciadv.1701290.

[28] J. Wu, M. Saito, M. Takeuchi, T. Watanabe, The stability of Cu/ZnO-based catalysts in methanol synthesis from a $CO_2$-rich feed and from a CO-rich feed, Appl. Catal., A Gen. 218 (2001) 235–240, https://doi.org/10.1016/S0926-860X(01)00650-0.

[29] M. Ao, G.H. Pham, J. Sunarso, M.O. Tade, S. Liu, Active centers of catalysts for higher alcohol synthesis from syngas: a review, ACS Catal. 8 (2018) 7025–7050, https://doi.org/10.1021/acscatal.8b01391.

[30] S.J. Han, G. Park, Y.J. Lee, K.W. Jun, S.K. Kim, Y.T. Kim, G. Kwak, Higher alcohol synthesis from syngas over xerogel-derived Co-Cu-$Al_2O_3$ catalyst with an enhanced metal proximity, Mol. Catal. 475 (2019), 110481, https://doi.org/10.1016/j.mcat.2019.110481.

[31] K. Bai, J. Huang, M. Tian, C. Han, W. Huang, Cerium doped Co/AC catalysts for higher alcohols synthesis from syngas, Mol. Catal. 546 (2023), 113270, https://doi.org/10.1016/j.mcat.2023.113270.

[32] F. Zeng, C. Mebrahtu, X. Xi, L. Liao, J. Ren, J. Xie, H.J. Heeres, R. Palkovits, Catalysts design for higher alcohols synthesis by $CO_2$ hydrogenation: Trends and future perspectives, Appl. Catal., B 291 (2021), 120073, https://doi.org/10.1016/j.apcatb.2021.120073.

[33] S. Liu, Y. He, W. Fu, J. Chen, J. Ren, L. Liao, R. Sun, Z. Tang, C. Mebrahtu, F. Zeng, Hetero-site cobalt catalysts for higher alcohols synthesis by $CO_2$ hydrogenation: A review, J. $CO_2$ Util. 67 (2023), 102322, https://doi.org/10.1016/j.jcou.2022.102322.

[34] D. Xu, Y. Wang, M. Ding, X. Hong, G. Liu, S.C.E. Tsang, Advances in higher alcohol synthesis from $CO_2$ hydrogenation, Chem 7 (2021) 849–881, https://doi.org/10.1016/j.chempr.2020.10.019.

[35] A.I. Latsiou, N.D. Charisiou, Z. Frontistis, A. Bansode, M.A. Goula, $CO_2$ hydrogenation for the production of higher alcohols: Trends in catalyst developments, challenges and opportunities, Catal. Today 420 (2023), 114179, https://doi.org/10.1016/J.CATTOD.2023.114179.

[36] G. Wang, R. Luo, C. Yang, J. Song, C. Xiong, H. Tian, Z.J. Zhao, R. Mu, J. Gong, Active sites in $CO_2$ hydrogenation over confined $VO_x$-Rh catalysts, Sci. China Chem. 62 (2019) 1710–1719, https://doi.org/10.1007/S11426-019-9590-6.

[37] H. Kusama, K. Okabe, K. Sayama, H. Arakawa, $CO_2$ hydrogenation to ethanol over promoted Rh/$SiO_2$ catalysts, Catal. Today 28 (1996) 261–266, https://doi.org/10.1016/0920-5861(95)00246-4.

[38] K. Zheng, Y. Li, B. Liu, F. Jiang, Y. Xu, X. Liu, Ti-doped $CeO_2$ stabilized single-atom rhodium catalyst for selective and stable $CO_2$ hydrogenation to ethanol, Angew. Chem. Int. Ed. 61 (2022), e202210991, https://doi.org/10.1002/anie.202210991.

[39] C. Yang, R. Mu, G. Wang, J. Song, H. Tian, Z.J. Zhao, J. Gong, Hydroxyl-mediated ethanol selectivity of $CO_2$ hydrogenation, Chem. Sci. 10 (2019) 3161–3167, https://doi.org/10.1039/c8sc05608k.

[40] M.R. Gogate, R.J. Davis, Comparative study of CO and $CO_2$ hydrogenation over supported Rh-Fe catalysts, Catal. Commun. 11 (2010) 901–906, https://doi.org/10.1016/j.catcom.2010.03.020.

[41] A. Goryachev, A. Pustovarenko, G. Shterk, N.S. Alhajri, A. Jamal, M. Albuali, L. van Koppen, I.S. Khan, A. Russkikh, A. Ramirez, T. Shoinkhorova, E.J. M. Hensen, J. Gascon, A multi-parametric catalyst screening for $CO_2$ hydrogenation to ethanol, ChemCatChem 13 (2021) 3324–3332, https://doi.org/10.1002/cctc.202100302.

[42] Y. Lou, F. jiang, W. Zhu, L. Wang, T. Yao, S. Wang, B. Yang, B. Yang, Y. Zhu, X. Liu, $CeO_2$ supported Pd dimers boosting $CO_2$ hydrogenation to ethanol, Appl. Catal., B 291 (2021), 120122, https://doi.org/10.1016/J.APCATB.2021.120122.

[43] S. Bai, Q. Shao, P. Wang, Q. Dai, X. Wang, X. Huang, Highly active and selective hydrogenation of $CO_2$ to ethanol by ordered Pd-Cu nanoparticles, J. Am. Chem. Soc. 139 (2017) 6827–6830, https://doi.org/10.1021/JACS.7B03101.

[44] F.J. Caparrós, L. Soler, M.D. Rossell, I. Angurell, L. Piccolo, O. Rossell, J. Llorca, Remarkable carbon dioxide hydrogenation to ethanol on a palladium/iron oxide single-atom catalyst, ChemCatChem 10 (2018) 2365–2369, https://doi.org/10.1002/cctc.201800362.

[45] Z. He, Q. Qian, J. Ma, Q. Meng, H. Zhou, J. Song, Z. Liu, B. Han, Water-enhanced synthesis of higher alcohols from $CO_2$ hydrogenation over a $Pt/Co_3O_4$ catalyst under milder conditions, Angew. Chem. Int. Ed. 55 (2016) 737–741, https://doi.org/10.1002/ANIE.201507585.

[46] B. Ouyang, S. Xiong, Y. Zhang, B. Liu, J. Li, The study of morphology effect of $Pt/Co_3O_4$ catalysts for higher alcohol synthesis from $CO_2$ hydrogenation, Appl. Catal., A Gen. 543 (2017) 189–195, https://doi.org/10.1016/j.apcata.2017.06.031.

[47] D. Wang, Q. Bi, G. Yin, W. Zhao, F. Huang, X. Xie, M. Jiang, Direct synthesis of ethanol via $CO_2$ hydrogenation using supported gold catalysts, Chem. Commun. 52 (2016) 14226–14229, https://doi.org/10.1039/c6cc08161d.

[48] X. Ye, C. Yang, X. Pan, J. Ma, Y. Zhang, Y. Ren, X. Liu, L. Li, Y. Huang, Highly selective hydrogenation of $CO_2$ to ethanol via designed bifunctional $Ir_1$-$In_2O_3$ single-atom catalyst, J. Am. Chem. Soc. 142 (2020) 19001–19005, https://doi.org/10.1021/JACS.0C08607.

[49] T. Witoon, T. Numpilai, S. Nijpanich, N. Chanlek, P. Kidkhunthod, C.K. Cheng, K. H. Ng, D.V.N. Vo, S. Ittisanronnachai, C. Wattanakit, M. Chareonpanich, J. Limtrakul, Enhanced $CO_2$ hydrogenation to higher alcohols over K-Co promoted $In_2O_3$ catalysts, Chem. Eng. J. 431 (2022), 133211, https://doi.org/10.1016/j.cej.2021.133211.

[50] S. Zhang, X. Liu, Z. Shao, H. Wang, Y. Sun, Direct $CO_2$ hydrogenation to ethanol over supported $Co_2C$ catalysts: Studies on support effects and mechanism, J. Catal. 382 (2020) 86–96, https://doi.org/10.1016/J.JCAT.2019.11.038.

[51] K. An, S. Zhang, J. Wang, Q. Liu, Z. Zhang, Y. Liu, A highly selective catalyst of $Co/La_4Ga_2O_9$ for $CO_2$ hydrogenation to ethanol, J. Energy Chem. 56 (2021) 486–495, https://doi.org/10.1016/j.jechem.2020.08.045.

[52] S. Zhang, Z. Wu, X. Liu, Z. Shao, L. Xia, L. Zhong, H. Wang, Y. Sun, Tuning the interaction between Na and $Co_2C$ to promote selective $CO_2$ hydrogenation to ethanol, Appl. Catal., B 293 (2021), 120207, https://doi.org/10.1016/J.APCATB.2021.120207.

[53] S. Zhang, C. Huang, Z. Shao, H. Zhou, J. Chen, L. Li, J. Lu, X. Liu, H. Luo, L. Xia, H. Wang, Y. Sun, Revealing and regulating the complex reaction mechanism of $CO_2$ hydrogenation to higher alcohols on multifunctional tandem catalysts, ACS Catal. 13 (2023) 3055–3065, https://doi.org/10.1021/ACSCATAL.2C06245.

[54] L. Wang, L. Wang, J. Zhang, X. Liu, H. Wang, W. Zhang, Q. Yang, J. Ma, X. Dong, S.J. Yoo, J.G. Kim, X. Meng, F.S. Xiao, Selective hydrogenation of $CO_2$ to ethanol over cobalt catalysts, Angew. Chem. Int. Ed. 57 (2018) 6104–6108, https://doi.org/10.1002/ANIE.201800729.

[55] L. Wang, S. He, L. Wang, Y. Lei, X. Meng, F.S. Xiao, Cobalt-Nickel catalysts for selective hydrogenation of carbon dioxide into ethanol, ACS Catal. 9 (2019) 11335–11340, https://doi.org/10.1021/acscatal.9b04187.

[56] B. Liu, B. Ouyang, Y. Zhang, K. Lv, Q. Li, Y. Ding, J. Li, Effects of mesoporous structure and Pt promoter on the activity of Co-based catalysts in low-temperature $CO_2$ hydrogenation for higher alcohol synthesis, J. Catal. 366 (2018) 91–97, https://doi.org/10.1016/j.jcat.2018.07.019.

[57] J. Zheng, K. An, J. Wang, J. Li, Y. Liu, Direct synthesis of ethanol via $CO_2$ hydrogenation over the Co/La-Ga-O composite oxide catalyst, J. Fuel Chem. Technol. 47 (2019) 697–708, https://doi.org/10.1016/S1872-5813(19)30031-3.

[58] S. Liu, H. Zhou, L. Zhang, Z. Ma, Y. Wang, Activated carbon-supported Mo-Co-K sulfide catalysts for synthesizing higher alcohols from $CO_2$, Chem. Eng. Technol. 42 (2019) 962–970, https://doi.org/10.1002/ceat.201800401.

[59] M. Irshad, H.J. Chun, M.K. Khan, H. Jo, S.K. Kim, J. Kim, Synthesis of *n*-butanol-rich $C_{3+}$ alcohols by direct $CO_2$ hydrogenation over a stable Cu–Co tandem catalyst, Appl. Catal., B. 340 (2024), 123201, https://doi.org/10.1016/j.apcatb.2023.123201.

[60] Y. Wang, K. Wang, B. Zhang, X. Peng, X. Gao, G. Yang, H. Hu, M. Wu, N. Tsubaki, Direct conversion of $CO_2$ to ethanol boosted by intimacy-sensitive multifunctional catalysts, ACS Catal. 11 (2021) 11742–11753, https://doi.org/10.1021/ACSCATAL.1C01504.

[61] T. Liu, D. Xu, M. Song, X. Hong, G. Liu, K-$ZrO_2$ interfaces boost $CO_2$ hydrogenation to higher alcohols, ACS Catal. 13 (2023) 4667–4674, https://doi.org/10.1021/acscatal.3c00074.

[62] B. An, Z. Li, Y. Song, J. Zhang, L. Zeng, C. Wang, W. Lin, Cooperative copper centres in a metal–organic framework for selective conversion of $CO_2$ to ethanol, Nat. Catal. 2 (2019) 709–717, https://doi.org/10.1038/s41929-019-0308-5.

[63] Y. Wang, X. Zhang, X. Hong, G. Liu, Sulfate-promoted higher alcohol synthesis from $CO_2$ hydrogenation, ACS Sustain. Chem. Eng. 10 (2022) 8980–8987, https://doi.org/10.1021/ACSSUSCHEMENG.2C02743.

[64] D. Xu, H. Yang, X. Hong, G. Liu, S.C. Edman Tsang, Tandem catalysis of direct $CO_2$ hydrogenation to higher alcohols, ACS Catal. 11 (2021) 8978–8984, https://doi.org/10.1021/acscatal.1c01610.

[65] D. Xu, M. Ding, X. Hong, G. Liu, Mechanistic aspects of the role of K promotion on Cu−Fe-based catalysts for higher alcohol synthesis from $CO_2$ hydrogenation, ACS Catal. 10 (2020) 14516–14526, https://doi.org/10.1021/ACSCATAL.0C03575.

[66] L. Ding, T. Shi, J. Gu, Y. Cui, Z. Zhang, C. Yang, T. Chen, M. Lin, P. Wang, N. Xue, L. Peng, X. Guo, Y. Zhu, Z. Chen, W. Ding, $CO_2$ hydrogenation to ethanol over Cu@Na-beta, Chem 6 (2020) 2673–2689, https://doi.org/10.1016/J.CHEMPR.2020.07.001.

[67] S.C. Qi, Z.H. Yang, R.R. Zhu, X.J. Lu, D.M. Xue, X.Q. Liu, L.B. Sun, The cascade catalysis of the porphyrinic zirconium metal–organic framework PCN-224-Cu for $CO_2$ conversion to alcohols, J. Mater. Chem. A 9 (2021) 24510–24516, https://doi.org/10.1039/D1TA06950K.

[68] C. Yang, S. Liu, Y. Wang, J. Song, G. Wang, S. Wang, Z. Zhao, R. Mu, J. Gong, The interplay between structure and product selectivity of $CO_2$ hydrogenation, Angew. Chem. Int. Ed. 131 (2019) 11364–11369, https://doi.org/10.1002/ange.201904649.

[69] H. Guo, S. Li, F. Peng, H. Zhang, L. Xiong, C. Huang, C. Wang, X. Chen, Roles Investigation of promoters in K/Cu-Zn catalyst and higher alcohols synthesis from $CO_2$ hydrogenation over a novel two-stage bed catalyst combination system, Catal. Lett. 145 (2015) 620–630, https://doi.org/10.1007/s10562-014-1446-7.

[70] X. Xi, F. Zeng, H. Zhang, X. Wu, J. Ren, T. Bisswanger, C. Stampfer, J.P. Hofmann, R. Palkovits, H.J. Heeres, $CO_2$ hydrogenation to higher alcohols over K-promoted bimetallic Fe−in catalysts on a Ce−$ZrO_2$ support, ACS Sustain. Chem. Eng. 9 (2021) 6235–6249, https://doi.org/10.1021/acssuschemeng.0c08760.

[71] Y. Chen, S. Choi, L.T. Thompson, Low temperature $CO_2$ hydrogenation to alcohols and hydrocarbons over $Mo_2C$ supported metal catalysts, J. Catal. 343 (2016) 147–156, https://doi.org/10.1016/j.jcat.2016.01.016.

[72] R. Yao, J. Wei, Q. Ge, J. Xu, Y. Han, Q. Ma, H. Xu, J. Sun, Monometallic iron catalysts with synergistic Na and S for higher alcohols synthesis via $CO_2$ hydrogenation, Appl. Catal., B 298 (2021), 120556, https://doi.org/10.1016/j.apcatb.2021.120556.

[73] L. Li, X. Li, Y. Sun, Y. Xie, Rational design of electrocatalytic carbon dioxide reduction for a zero-carbon network, Chem. Soc. Rev. 51 (2022) 1234–1252, https://doi.org/10.1039/d1cs00893e.

[74] L. Falivene, S.M. Kozlov, L. Cavallo, Constructing bridges between computational tools in heterogeneous and homogeneous catalysis, ACS Catal. 8 (2018) 5637–5656, https://doi.org/10.1021/acscatal.8b00042.

[75] K. McCullough, T. Williams, K. Mingle, P. Jamshidi, J. Lauterbach, High-throughput experimentation meets artificial intelligence: A new pathway to catalyst discovery, Phys. Chem. Chem. Phys. 22 (2020) 11174–11196, https://doi.org/10.1039/d0cp00972e.

[76] T. Jaster, A. Gawel, D. Siegmund, J. Holzmann, H. Lohmann, E. Klemm, U. P. Apfel, Electrochemical $CO_2$ reduction toward multicarbon alcohols - The microscopic world of catalysts & process conditions, iScience 25 (2022), 104010, https://doi.org/10.1016/j.isci.2022.104010.

[77] H.Y.T. Chen, S. Tosoni, G. Pacchioni, Hydrogen adsorption, dissociation, and spillover on $Ru_{10}$ clusters supported on anatase $TiO_2$ and tetragonal $ZrO_2$ (101) surfaces, ACS Catal. 5 (2015) 5486–5495, https://doi.org/10.1021/acscatal.5b01093.

[78] D.R. Aireddy, K. Ding, Heterolytic dissociation of $H_2$ in heterogeneous catalysis, ACS Catal. 12 (2022) 4707–4723, https://doi.org/10.1021/ACSCATAL.2C00584.

[79] S.E. Collins, M.A. Baltanás, A.L. Bonivardi, An infrared study of the intermediates of methanol synthesis from carbon dioxide over Pd/β-$Ga_2O_3$, J. Catal. 226 (2004) 410–421, https://doi.org/10.1016/J.JCAT.2004.06.012.

[80] S.E. Collins, J.J. Delgado, C. Mira, J.J. Calvino, S. Bernal, D.L. Chiavassa, M. A. Baltanás, A.L. Bonivardi, The role of Pd–Ga bimetallic particles in the bifunctional mechanism of selective methanol synthesis via $CO_2$ hydrogenation on a Pd/$Ga_2O_3$ catalyst, J. Catal. 292 (2012) 90–98, https://doi.org/10.1016/J.JCAT.2012.05.005.

[81] K. Lee, U. Anjum, T.P. Araújo, C. Mondelli, Q. He, S. Furukawa, J. Pérez-Ramírez, S.M. Kozlov, N. Yan, Atomic Pd-promoted $ZnZrO_x$ solid solution catalyst for $CO_2$ hydrogenation to methanol, Appl. Catal., B 304 (2022), 120994, https://doi.org/10.1016/j.apcatb.2021.120994.

[82] N. Yodsin, C. Rungnim, S. Tungkamani, V. Promarak, S. Namuangruk, S. Jungsuttiwong, DFT study of catalytic $CO_2$ hydrogenation over Pt-decorated carbon nanocones: $H_2$ dissociation combined with the spillover mechanism, J. Phys. Chem. C. 124 (2020) 1941–1949, https://doi.org/10.1021/acs.jpcc.9b08776.

[83] L. Song, H. Wang, S. Wang, Z. Qu, Dual-site activation of $H_2$ over Cu/$ZnAl_2O_4$ boosting $CO_2$ hydrogenation to methanol, Appl. Catal., B 322 (2023), 122137, https://doi.org/10.1016/j.apcatb.2022.122137.

[84] W. Liao, C. Tang, H. Zheng, J. Ding, K. Zhang, H. Wang, J. Lu, W. Huang, Z. Zhang, Tuning activity and selectivity of $CO_2$ hydrogenation via metal-oxide interfaces over ZnO-supported metal catalysts, J. Catal. 407 (2022) 126–140, https://doi.org/10.1016/j.jcat.2022.01.037.

[85] L.L. Ling, W. Yang, P. Yan, M. Wang, H.L. Jiang, Light-assisted $CO_2$ hydrogenation over $Pd_3Cu$@UiO-66 promoted by active sites in close proximity, Angew. Chem. Int. Ed. 61 (2022), e202116396, https://doi.org/10.1002/ANIE.202116396.

[86] K. Lee, P.C.D. Mendes, H. Jeon, Y. Song, M.P. Dickieson, U. Anjum, L. Chen, T. C. Yang, C.M. Yang, M. Choi, S.M. Kozlov, N. Yan, Engineering nanoscale H supply chain to accelerate methanol synthesis on $ZnZrO_x$, Nat. Commun. 14 (2023), 819, https://doi.org/10.1038/s41467-023-36407-1.

[87] H.T. Luk, C. Mondelli, S. Mitchell, S. Siol, J.A. Stewart, D. Curulla Ferré, J. Pérez-Ramírez, Role of carbonaceous supports and potassium promoter on higher alcohols synthesis over copper-iron catalysts, ACS Catal. 8 (2018) 9604–9618, https://doi.org/10.1021/ACSCATAL.8B02714.

[88] R. Xu, Z. Ma, C. Yang, W. Wei, Y. Sun, Influence of promoter on catalytic properties of Cu-Mn-Fe/$ZrO_2$ catalysts for alcohols synthesis, React. Kinet. Catal. Lett. 81 (2004) 91–98, https://doi.org/10.1023/B:REAC.0000016521.91502.5F.

[89] M. Ding, L. Ma, Q. Zhang, C. Wang, W. Zhang, T. Wang, Enhancement of conversion from bio-syngas to higher alcohols fuels over K-promoted Cu-Fe bimodal pore catalysts, Fuel Process. Technol. 159 (2017) 436–441, https://doi.org/10.1016/J.FUPROC.2017.02.010.

[90] M. Ding, J. Tu, M. Qiu, T. Wang, L. Ma, Y. Li, Impact of potassium promoter on Cu–Fe based mixed alcohols synthesis catalyst, Appl. Energy 138 (2015) 584–589, https://doi.org/10.1016/J.APENERGY.2014.01.010.

[91] N. Zou, J. Chen, T. Qiu, Y. Zheng, Direct hydrogenation of $CO_2$ to ethanol at ambient conditions using Cu(I)-MOF in a dielectric barrier discharge plasma reactor, J. Mater. Chem. A 11 (2023) 10766–10775, https://doi.org/10.1039/D3TA00314K.

[92] R.P. Ye, J. Ding, W. Gong, M.D. Argyle, Q. Zhong, Y. Wang, C.K. Russell, Z. Xu, A. G. Russell, Q. Li, M. Fan, Y.G. Yao, $CO_2$ hydrogenation to high-value products via heterogeneous catalysis, Nat. Commun. 10 (2019), 5698, https://doi.org/10.1038/s41467-019-13638-9.

[93] X. Nie, X. Jiang, H. Wang, W. Luo, M.J. Janik, Y. Chen, X. Guo, C. Song, Mechanistic understanding of alloy effect and water promotion for Pd-Cu bimetallic catalysts in $CO_2$ hydrogenation to methanol, ACS Catal. 8 (2018) 4873–4892, https://doi.org/10.1021/ACSCATAL.7B04150.

[94] Y.P. Pei, J.X. Liu, Y.H. Zhao, Y.J. Ding, T. Liu, W.Da Dong, H.J. Zhu, H.Y. Su, L. Yan, J.L. Li, W.X. Li, High alcohols synthesis via fischer-tropsch reaction at cobalt metal/carbide interface, ACS Catal. 5 (2015) 3620–3624, https://doi.org/10.1021/acscatal.5b00791.

[95] X.C. Xu, J. Su, P. Tian, D. Fu, W. Dai, W. Mao, W.K. Yuan, J. Xu, Y.F. Han, First-principles study of $C_2$ oxygenates synthesis directly from syngas over CoCu bimetallic catalysts, J. Phys. Chem. C. 119 (2015) 216–227, https://doi.org/10.1021/JP5065159.

[96] H. Liang, B. Zhang, P. Gao, X. Yu, X. Liu, X. Yang, H. Wu, L. Zhai, S. Zhao, G. Wang, A.P. van Bavel, Y. Qin, Strong Co-O-Si bonded ultra-stable single-atom Co/SBA-15 catalyst for selective hydrogenation of $CO_2$ to CO, Chem. Catal. 2 (2022) 610–621, https://doi.org/10.1016/j.checat.2022.01.020.

[97] T. Lin, X. Qi, X. Wang, L. Xia, C. Wang, F. Yu, H. Wang, S. Li, L. Zhong, Y. Sun, Direct production of higher oxygenates by syngas conversion over a multifunctional catalyst, Angew. Chem. Int. Ed. 58 (2019) 4627–4631, https://doi.org/10.1002/ANIE.201814611.

[98] C. Huang, C. Zhu, M. Zhang, Y. Lu, Q. Wang, H. Qian, J. Chen, K. Fang, Direct conversion of syngas to higher alcohols over a CuCoAl|t-$ZrO_2$ multifunctional catalyst, ChemCatChem 13 (2021) 3184–3197, https://doi.org/10.1002/CCTC.202100293.

[99] K. Sun, Y. Wu, M. Tan, L. Wang, G. Yang, M. Zhang, W. Zhang, Y. Tan, Ethanol and higher alcohols synthesis from syngas over CuCoM (M=Fe, Cr, Ga and Al) nanoplates derived from hydrotalcite-like precursors, ChemCatChem 11 (2019) 2695–2706, https://doi.org/10.1002/CCTC.201900096.

[100] I.C. ten Have, J.J.G. Kromwijk, M. Monai, D. Ferri, E.B. Sterk, F. Meirer, B. M. Weckhuysen, Uncovering the reaction mechanism behind CoO as active phase for $CO_2$ hydrogenation, Nat. Commun. 13 (2022), 324, https://doi.org/10.1038/s41467-022-27981-x.

[101] H.T. Luk, C. Mondelli, D.C. Ferré, J.A. Stewart, J. Pérez-Ramírez, Status and prospects in higher alcohols synthesis from syngas, Chem. Soc. Rev. 46 (2017) 1358–1426, https://doi.org/10.1039/C6CS00324A.

[102] N.D. Subramanian, J. Gao, X. Mo, J.G. Goodwin, W. Torres, J.J. Spivey, La and/or V oxide promoted Rh/$SiO_2$ catalysts: Effect of temperature, $H_2$/CO ratio, space velocity, and pressure on ethanol selectivity from syngas, J. Catal. 272 (2010) 204–209, https://doi.org/10.1016/J.JCAT.2010.03.019.

[103] J.J. Spivey, A. Egbebi, Heterogeneous catalytic synthesis of ethanol from biomass-derived syngas, Chem. Soc. Rev. 36 (2007) 1514–1528, https://doi.org/10.1039/B414039G.

[104] D.C. Grinter, J. Graciani, R.M. Palomino, F. Xu, I. Waluyo, J.F. Sanz, S. D. Senanayake, J.A. Rodriguez, Adsorption and activation of $CO_2$ on Pt/$CeO_x$/$TiO_2$(110): Role of the Pt-$CeO_x$ interface, Surf. Sci. 710 (2021), 121852, https://doi.org/10.1016/J.SUSC.2021.121852.

[105] J. Graciani, D.C. Grinter, P.J. Ramírez, R.M. Palomino, F. Xu, I. Waluyo, D. Stacchiola, J.F. Sanz, S.D. Senanayake, J.A. Rodriguez, Conversion of $CO_2$ to methanol and ethanol on Pt/$CeO_x$/$TiO_2$(110): enabling role of water in C-C bond formation, ACS Catal. 12 (2022) 15097–15109, https://doi.org/10.1021/ACSCATAL.2C03823.

[106] Y. Zhao, C. Cui, J. Han, H. Wang, X. Zhu, Q. Ge, Direct C-C Coupling of $CO_2$ and the methyl group from $CH_4$ activation through facile insertion of $CO_2$ into Zn-$CH_3$ σ-Bond, J. Am. Chem. Soc. 138 (2016) 10191–10198, https://doi.org/10.1021/JACS.6B04446.

[107] M. Zhang, R. Yao, H. Jiang, G. Li, Y. Chen, Insights into the mechanism of acetic acid hydrogenation to ethanol on Cu(111) surface, Appl. Surf. Sci. 412 (2017) 342–349, https://doi.org/10.1016/J.APSUSC.2017.03.222.

[108] Y. Izumi, Selective ethanol synthesis from carbon dioxide, Platin. Met. Rev. 41 (1997) 166–170.

[109] G. Wang, R. Zhang, B. Wang, Insight into the preference mechanism for C–C chain formation of $C_2$ oxygenates and the effect of promoters in syngas conversion over Cu-based catalysts, Appl. Catal., A 466 (2013) 77–89, https://doi.org/10.1016/J.APCATA.2013.06.042.

[110] B. Ren, X. Dong, Y. Yu, G. Wen, M. Zhang, A density functional theory study on the carbon chain growth of ethanol formation on Cu-Co (111) and (211) surfaces, Appl. Surf. Sci. 412 (2017) 374–384, https://doi.org/10.1016/J.APSUSC.2017.03.106.

[111] C. Wang, J. Zhang, G. Qin, L. Wang, E. Zuidema, Q. Yang, S. Dang, C. Yang, J. Xiao, X. Meng, C. Mesters, F.S. Xiao, Direct conversion of syngas to ethanol within zeolite crystals, Chem 6 (2020) 646–657, https://doi.org/10.1016/j.chempr.2019.12.007.

[112] X. Sun, R. Zhang, B. Wang, Insights into the preference of $CH_x$(x = 1–3) formation from CO hydrogenation on Cu(111) surface, Appl. Surf. Sci. 265 (2013) 720–730, https://doi.org/10.1016/J.APSUSC.2012.11.091.

[113] R. Zhang, X. Sun, B. Wang, Insight into the preference mechanism of $CH_x$ (x = 1–3) and C–C chain formation involved in $C_2$ oxygenate formation from syngas on the Cu(110) surface, J. Phys. Chem. C. 117 (2013) 6594–6606, https://doi.org/10.1021/JP311701R.

[114] H. Zheng, R. Zhang, Z. Li, B. Wang, Insight into the mechanism and possibility of ethanol formation from syngas on Cu(1 0 0) surface, J. Mol. Catal. A: Chem. 404–405 (2015) 115–130, https://doi.org/10.1016/J.MOLCATA.2015.04.015.

[115] R. Zhang, G. Wang, B. Wang, L. Ling, Insight into the effect of promoter Mn on ethanol formation from syngas on a Mn-promoted MnCu(211) surface: A comparison with a Cu(211) surface, J. Phys. Chem. C. 118 (2014) 5243–5254, https://doi.org/10.1021/JP409447U.

[116] R. Zhang, G. Wang, B. Wang, Insights into the mechanism of ethanol formation from syngas on Cu and an expanded prediction of improved Cu-based catalyst, J. Catal. 305 (2013) 238–255, https://doi.org/10.1016/J.JCAT.2013.05.028.

[117] W. Wang, Y. Wang, G.C. Wang, Ethanol synthesis from syngas over Cu(Pd)-doped Fe(100): a systematic theoretical investigation, Phys. Chem. Chem. Phys. 20 (2018) 2492–2507, https://doi.org/10.1039/C7CP06693G.

[118] X. Wang, P.J. Ramírez, W. Liao, J.A. Rodriguez, P. Liu, Cesium-induced active sites for C–C coupling and ethanol synthesis from $CO_2$ hydrogenation on Cu/ZnO ($000\bar{1}$) surfaces, J. Am. Chem. Soc. 143 (2021) 13103–13112, https://doi.org/10.1021/JACS.1C03940.

[119] R. Zhang, Y. Wang, P. Gaspard, N. Kruse, The oscillating Fischer-Tropsch reaction, Science 382 (2023) 99–103, https://doi.org/10.1126/science.adh8463.

[120] S. Wu, N. Salmon, M.M.J. Li, R. Bañares-Alcántara, S.C.E. Tsang, Energy decarbonization via green $H_2$ or $NH_3$? ACS Energy Lett. 7 (2022) 1021–1033, https://doi.org/10.1021/acsenergylett.1c02816.

[121] W. Xue, J. Wang, H. Huang, Y. Cui, D. Mei, CO oxidation over HKUST-1 catalysts: The role of defective sites, J. Phys. Chem. C. 126 (2022) 9652–9664, https://doi.org/10.1021/ACS.JPCC.2C01022.

[122] P. Gao, L. Zhang, S. Li, Z. Zhou, Y. Sun, Novel heterogeneous catalysts for $CO_2$ hydrogenation to liquid fuels, ACS Cent. Sci. 6 (2020) 1657–1670, https://doi.org/10.1021/acscentsci.0c00976.

[123] P. Liu, Y. Yang, M.G. White, Theoretical perspective of alcohol decomposition and synthesis from $CO_2$ hydrogenation, Surf. Sci. Rep. 68 (2013) 233–272, https://doi.org/10.1016/j.surfrep.2013.01.001.

[124] J. Chen, Y. Zha, B. Liu, Y. Li, Y. Xu, X. Liu, Rationally designed water enriched nano reactor for stable $CO_2$ hydrogenation with near 100% ethanol selectivity over diatomic palladium active sites, ACS Catal. (2023) 7110–7121, https://doi.org/10.1021/acscatal.3c00586.

[125] Z.W. Ulissi, A.J. Medford, T. Bligaard, J.K. Nørskov, To address surface reaction network complexity using scaling relations machine learning and DFT calculations, Nat. Commun. 8 (2017), 14621, https://doi.org/10.1038/ncomms14621.

[126] M. Suvarna, T.P. Araújo, J. Pérez-Ramírez, A generalized machine learning framework to predict the space-time yield of methanol from thermocatalytic $CO_2$ hydrogenation, Appl. Catal., B. 315 (2022), 121530, https://doi.org/10.1016/j.apcatb.2022.121530.

[127] M. Suvarna, P. Preikschas, J. Perez-Ramirez, Identifying descriptors for promoted Rhodium-based catalysts for higher alcohol synthesis via machine learning, ACS Catal. 12 (2022) 15373–15385, https://doi.org/10.1021/ACSCATAL.2C04349.

[128] K. Tripathi, V. Gupta, V. Awasthi, K.K. Pant, S. Upadhyayula, Forecasting catalytic property-performance correlations for $CO_2$ hydrogenation to methanol via surrogate machine learning framework, Adv. Sustain. Syst. 7 (2023), 2200416, https://doi.org/10.1002/ADSU.202200416.

[129] Y.F. Shi, P.L. Kang, C. Shang, Z.P. Liu, Methanol synthesis from $CO_2$/CO mixture on Cu-Zn catalysts from microkinetics-guided machine learning pathway search, J. Am. Chem. Soc. 144 (2022) 13401–13414, https://doi.org/10.1021/JACS.2C06044.

[130] J. Behler, Perspective: Machine learning potentials for atomistic simulations, J. Chem. Phys. 145 (2016), 170901, https://doi.org/10.1063/1.4966192/195141.

[131] P.L. Kang, C. Shang, Z.P. Liu, Large-scale atomic simulation via machine learning potentials constructed by global potential energy surface exploration, Acc. Chem. Res. 53 (2020) 2119–2129, https://doi.org/10.1021/ACS.ACCOUNTS.0C00472.

[132] B. Mortazavi, X. Zhuang, T. Rabczuk, A.V. Shapeev, Atomistic modeling of the mechanical properties: the rise of machine learning interatomic potentials, Mater. Horiz. 10 (2023) 1956–1968, https://doi.org/10.1039/D3MH00125C.

[133] D. Chen, C. Shang, Z.P. Liu, Machine-learning atomic simulation for heterogeneous catalysis, npj Comput. Mater. 9 (2023), 2, https://doi.org/10.1038/s41524-022-00959-5.

[134] V.L. Deringer, M.A. Caro, G. Csányi, Machine learning interatomic potentials as emerging tools for materials science, Adv. Mater. 31 (2019), 1902765, https://doi.org/10.1002/ADMA.201902765.

[135] A. Jain, S.P. Ong, G. Hautier, W. Chen, W.D. Richards, S. Dacek, S. Cholia, D. Gunter, D. Skinner, G. Ceder, K.A. Persson, Commentary: The materials project: A materials genome approach to accelerating materials innovation, APL Mater. 1 (2013) 11002.

[136] S. Kirklin, J.E. Saal, B. Meredig, A. Thompson, J.W. Doak, M. Aykol, S. Rühl, C. Wolverton, The open quantum materials database (OQMD): assessing the accuracy of DFT formation energies, npj Comput. Mater. 1 (2015) 1–15, https://doi.org/10.1038/npjcompumats.2015.10.

[137] J.E. Saal, S. Kirklin, M. Aykol, B. Meredig, C. Wolverton, Materials design and discovery with high-throughput density functional theory: The open quantum materials database (OQMD), JOM 65 (2013) 1501–1509, https://doi.org/10.1007/S11837-013-0755-4.

[138] C. Draxl, M. Scheffler, NOMAD: The FAIR concept for big data-driven materials science, MRS Bull. 43 (2018) 676–682, https://doi.org/10.1557/MRS.2018.208.

[139] D.D. Landis, J.S. Hummelshøj, S. Nestorov, J. Greeley, M. Dułłak, T. Bligaard, J. K. Nørskov, K.W. Jacobsen, The computational materials repository, Comput. Sci. Eng. 14 (2012) 51–57, https://doi.org/10.1109/MCSE.2012.16.
[140] J.S. Hummelshøj, F. Abild-Pedersen, F. Studt, T. Bligaard, J.K. Nørskov, CatApp: A web application for surface chemistry and heterogeneous catalysis, Angew. Chem. Int. Ed. 51 (2012) 272–274, https://doi.org/10.1002/ANIE.201107947.
[141] L. Chanussot, A. Das, S. Goyal, T. Lavril, M. Shuaibi, M. Riviere, K. Tran, J. Heras-Domingo, C. Ho, W. Hu, A. Palizhati, A. Sriram, B. Wood, J. Yoon, D. Parikh, C. L. Zitnick, Z. Ulissi, Open catalyst 2020 (OC20) dataset and community challenges, ACS Catal. 11 (2021) 6059–6072, https://doi.org/10.1021/ACSCATAL.0C04525.
[142] K.T. Winther, M.J. Hoffmann, J.R. Boes, O. Mamun, M. Bajdich, T. Bligaard, Catalysis-Hub.org, an open electronic structure database for surface reactions, 2019 6:1, Sci. Data 6 (2019) 1–10, https://doi.org/10.1038/s41597-019-0081-y.
[143] Z.J. Zhao, S. Liu, S. Zha, D. Cheng, F. Studt, G. Henkelman, J. Gong, Theory-guided design of catalytic materials using scaling relationships and reactivity descriptors, Nat. Rev. Mater. 4 (2019) 792–804, https://doi.org/10.1038/s41578-019-0152-x.
[144] R. Laplaza, S. Das, M.D. Wodrich, C. Corminboeuf, Constructing and interpreting volcano plots and activity maps to navigate homogeneous catalyst landscapes, Nat. Protoc. 17 (2022) 2550–2569, https://doi.org/10.1038/s41596-022-00726-2.
[145] S. Pablo-García, S. Morandi, R.A. Vargas-Hernández, K. Jorner, Ž. Ivković, N. López, A. Aspuru-Guzik, Fast evaluation of the adsorption energy of organic molecules on metals via graph neural networks, Nat. Comput. Sci. 3 (2023) 433–442, https://doi.org/10.1038/s43588-023-00437-y.
[146] W. Xu, Tailoring complexity for catalyst discovery using physically motivated machine learning, Technische Universität München, 2022.
[147] M. Zhong, K. Tran, Y. Min, C. Wang, Z. Wang, C.T. Dinh, P. De Luna, Z. Yu, A. S. Rasouli, P. Brodersen, S. Sun, O. Voznyy, C.S. Tan, M. Askerka, F. Che, M. Liu, A. Seifitokaldani, Y. Pang, S.C. Lo, A. Ip, Z. Ulissi, E.H. Sargent, Accelerated discovery of $CO_2$ electrocatalysts using active machine learning, Nature 581 (2020) 178–183, https://doi.org/10.1038/s41586-020-2242-8.
[148] Y. Chen, Y. Huang, T. Cheng, W.A. Goddard, Identifying active sites for $CO_2$ reduction on dealloyed gold surfaces by combining machine learning with multiscale simulations, J. Am. Chem. Soc. 141 (2019) 11651–11657, https://doi.org/10.1021/JACS.9B04956.
[149] D. Roy, S.C. Mandal, B. Pathak, Machine learning-driven high-throughput screening of alloy-based catalysts for selective $CO_2$ hydrogenation to methanol, ACS Appl. Mater. Interfaces 13 (2021) 56151–56163, https://doi.org/10.1021/ACSAMI.1C16696.
[150] D. Roy, S.C. Mandal, B. Pathak, Machine learning assisted exploration of high entropy alloy-based catalysts for selective $CO_2$ reduction to methanol, J. Phys. Chem. Lett. 13 (2022) 5991–6002, https://doi.org/10.1021/ACS.JPCLETT.2C00929.
[151] Z.W. Chen, Z. Gariepy, L. Chen, X. Yao, A. Anand, S.J. Liu, C.G. Tetsassi Feugmo, I. Tamblyn, C.V. Singh, Machine-learning-driven high-entropy alloy catalyst discovery to circumvent the scaling relation for $CO_2$ reduction reaction, ACS Catal. 12 (2022) 14864–14871, https://doi.org/10.1021/ACSCATAL.2C03675.